國立臺灣大學工學院機械工程學研究所

碩士論文

Department of Mechanical Engineering

College of Engineering

Natural Taiwan University

Master Thesis

奈米碳管印製於紅銅圓柱表面之冷凝熱傳研究

Experimental Investigation of Condensation Heat

Transfer on a CNT Printed Copper Cylinder

劉家齊

Chia-Chi Liu

指導教授: 陳炳煇　博士

Advisor: Ping-Hei Chen, Ph.D.

中華民國 108 年 7 月

July, 2019

(附件 3)

國立臺灣大學（碩）博士學位論文
口試委員會審定書

奈米碳管印製於紅銅圓柱表面之冷凝熱傳研究

Experimental Investigation of Condensation Heat Transfer on CNT Printed Copper Cylinder

本論文係劉家齊君（學號 R06522108）在國立臺灣大學機械工程學系、所完成之碩（博）士學位論文，於民國 108 年 7 月 17 日承下列考試委員審查通過及口試及格，特此證明

口試委員：

＿＿＿＿＿＿＿＿＿＿＿＿＿＿＿＿＿＿＿＿（簽名）
（指導教授）

＿＿＿＿＿＿＿＿＿＿＿　＿＿＿＿＿＿＿＿＿＿＿

＿＿＿＿＿＿＿＿＿＿＿　＿＿＿＿＿＿＿＿＿＿＿

系主任、所長　＿＿＿＿＿＿＿＿＿＿＿　（簽名）

（是否須簽章依各院系所規定）

致謝

　　兩年的碩士生活一轉眼就過去了，這段期間在台大和台北的生活著實讓我充實不少。首先感謝我的家人，給予我能安心在台北好好念書的資源，一路上的栽培讓我萬分感激。感謝老師兩年給予的建議，不論是研究上還是其他方面皆有所收穫。感謝實驗室學長們的幫助，每一次的 meeting 讓我逐步了解自己在研究過程中的每一項細節。感謝上一屆的學長姐們，以及同屆的夥伴們：戴耀俞、王裕翔、陳德璇，彼此互相激勵讓我度過多道困進。特別感謝馬里歐，除了平常的鼓勵外，也會偶爾聊聊生活瑣事，為我的研究生活添增幾分色彩。感謝實驗室的學弟們，在碩士最後一年多了些許趣味。

　　感謝台大擊劍隊的每一位夥伴，能成為隊上一份子一起參與訓練，並為校爭光，我深感驕傲；特此感謝同劍種優秀的學弟們，我很慶幸在台大終於在擊劍領域有所成就。感謝台大網球社，讓我重拾網球的樂趣，並明顯感覺自己的球技的提升，每一次的練球都是我做為碩士生的一項目標。感謝在台北生活期間認識的每一個人，讓我在台北多了份聯繫的情誼。最後感謝過去的自己，每一次選擇或許不一定都有好的結果，但正因為過去才有現今的我。

中文摘要

　　本研究探討在密閉腔體下的冷凝熱傳現象。以外直徑 25mm 的紅銅館為熱傳導物質，利用較為簡單的印製方式在紅銅柱表面印上奈米碳管墨，以不同印製面積比當作變因，也就是比較純紅銅、全冷凝表面印製、30%、50%、70%，進行實驗觀測該印製的奈米碳管對於冷凝現象的影像。

　　經量測顯示奈米碳管印製面積的接觸角為 76°，而未改質表面之接觸角為 107°，然而實驗結果觀測到，在低過冷度段，也就是 0~7.5°，印製面積 30% 和 50% 均有呈現熱傳增強的現象，經影像觀測發現在此過冷度區間不分親水性面積有助於冷凝液的移動和成核。而過冷度大於 7.5°，也就是近濕潤轉變後，印製面積 30%、50%、70% 的熱傳效果有降低的趨勢。由此研究可得知，此方法印製的奈米碳管表面會呈現親水性，但部分印製的冷凝表面再低過冷度區間有熱傳增強的效果。

關鍵字: 冷凝熱傳、表面改質、濕潤性、奈米碳管、紅銅柱

Abstract

This research focused on condensation heat transfer of copper cylinder inside a closed chamber. The dimension of cylinder is 25mm in diameter and 50mm in length. Besides, the modification method is printing carbon nanotube (CNT) onto the copper surface with different printing area ratio: 0%, 30%, 50%, 70%, and 100% as one of controlling factors. The other one is the subcooling degree, which is the temperature difference between condensation wall and steam.

After measurement, the wettability of CNT printed area is hydrophilic, while the one of plain surface is hydrophobic. However, the experimental results showed that within lower interval of subcooling degrees, which is 0 to 7.5°, the heat transfer coefficient and heat flux of the 30% and the 50% types are higher than the plain one. Accompanying the experimental images, hydrophilic surface has benefit to droplet movement and nucleation. On the other hands, the 30%, the 50%, and the 70% types worsen the heat transfer as the subcooling degree is >7.5° because the wetting transition induced the flooding upon the surface. From this research, even with hydrophilic patterns, the heat transfer performance could be enhanced during some subcooling degrees.

Keywords: condensation heat transfer, surface modification, wettability, carbon nanotube, copper cylinder

Nomenclature

A_{cross}	Cross section area of copper cylinder
A_0	Unmodified area
A_m	Modified area
A_{total}	Total area of condensation
C	Molecular concentration
C_P	Specific heat
D	Diameter of copper cylinder
ΔG	Energy barrier of nucleation
H	Height of microstructure
h_{cond}	Heat transfer coefficient of condensation
h_{lv}	Latent heat of water evaporation
J	Nucleation speed
J_d	Nucleation flux
k_{copper}	Thermal conductivity of copper
k_b	Boltzmann constant
L	Copper length
l	Half length of unprinted area
m	Length of printed area
$\dot{m}$	Mass flow rate of cooling water
P_v	Vapor pressure
P_{sat}	Satruation pressure
P_c	Critical pressure
Q_{water}	Heat taken by cooling water
$Q_{lateral}$	Heat transporting in lateral direction
q_{avg}	Average heat flux
R	Roughness
r	Radius of droplet
r_e	Minimum radius of nucleation
r_{max}	Radius of removal
T_{sat}	Saturation temperature
T_w	Surface temperature of copper cylinder
T_{left}	Average temperature on left side
T_{right}	Average temperature on right side
T_{outlet}	Temperature of water outlet
T_{inlet}	Temperature of water inlet
T_v	Vapor temperature

VI

T_{sub}	Subcooling degree
t	time
v_l	water specific volume
W	Ratio of non condensable gas
W_{tr}	Energy barrier of wetting transition
α	Angle
β	Angle
$\emptyset$	Angle
θ_{We}	Contact angle of Wenzel model
θ_{CB}	Contact angle of Cassie Baxter model
φ_s	Ratio of droplet contacting onto substrate surface
ρ	Density
σ	Surface tention

Content

List of Figures

X

List of Tables

Chapter 1. Introduction

1.1 Motivation

Condensation heat transfer has been widespread applied in various industries

including desalination [1], power generation [2], air conditioners [3], and etc. There

are types of condensation. The filmwise condensation is tha the vapor forms liquid

films on the surface, while the dropwise condensation shows little droplets emerge on

the surface. Researches have indicated that the heat transfer performance in dropwise

condensation is better than filmwise condensation [4, 5], which results from the lower

surface energy between the substrate and water. As the wettability of the surface is

more hydrophobic, droplets can be removed more easily, allowing the next occurrence

of condensation, leading to the enhancement in heat transfer rate. From this aspect,

the central target is to use surface modification to change the wettability [6],

manipulating the distribution of different wettability patterns [7, 8], and making a

microstructure on surface [9]. On the other hands, carbon nanotube (CNT), which is a

hollow-cylinder shape composed of a two-dimensional hexagonal lattice of carbon

atoms, attracts attention in this decade for its excellent physical properties, such as

electric conductivity, thermal conductivity, and stiffness and stress. In general, CNT is

used in the conductive materials in electrical circuit [10], and composition material

[11]. However, most researches applied complex methods to modify CNT.

1

Inspired by the pioneers, my motivation is to combine the condensation with simple methods of print CNT, and investigate the heat transfer phenomenon.

2

1.2 Literature Review
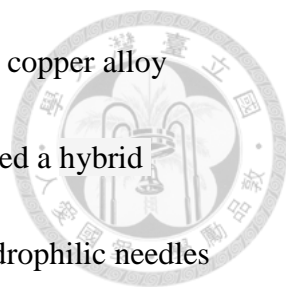
1.2.1 Condensation Heat Transfer Enhancement

The experiment on dropwise condensation have been conducted since 1930.

Schmidt indicated that the heat transfer coefficient of dropwise condensation was one

order higher in magnitude than filmwise condensation [4]. However, The theory of

dropwise condensation is studied until 1960s, suggested by Le Fevre et a [12]. In

1999, Rose et al made a conclusion that the heat transfer coefficient of dropwise

condensation is ten to twenty times than it of filmwise condensation [13]. Due to its

potential, numerous researchers devoted themselves into enhancing dropwise

condensation by employing surface modification. Besides, lotus surface, which shown

as Figure 1-1 [14], has inspired researchers of the investigation and manufacture of

superhydrophobic surfaces. To sum up, the hydrophobic surface can be achieved by

ion plating [15], lithography [16], chemical vapor deposition [17], layer-by-layer

deposition [18], and chemical coating [19-23].

Among these modified methods, some focused on maintaining the dropwise

condensation condition. Vemuri et al used self-assembled monolayer of n-octadecyl

mercaptan to produce a hydrophobic surface, showing as Figure 1-2 [24, 25], and

found that the condensation heat transfer coefficient SAM (n-octadecyl mercaptan)

coating increased by a factor of approximately 3 after 100 h of experimentation, and

3

by a factor of approximately 1.8 after 2600 h of experimentation for copper alloy

surfaces, under vacuum condition in 33.86 kPa. Mondal et al designed a hybrid

superhydrophobic–hydrophilic surface, composed of an array of hydrophilic needles

on superhydrophobic surface, monitored the droplet growth rate, and demonstrated

the 26 and 28 hours wetting condition in Figure 1-3 [26]. Moreover, in Shim et al's

study, a cerium-oxide material was investigated as modified surface on copper, in to

improve the thermal stability [27]. Shim et al concluded that after 12 hours test of

exposure to the hot steam condition, the cerium-oxide surfaces can remain its original

microscope condensation behaviors, leading to stable heat transfer performance

compared with the substrate treated with FAS-17

(1H,1H,2H,2H-perfluorodecyltrimethoxysilane) coating, as in Figure 1-4.

In spite of the experimental methods related to the maintenance of hydrophobic

surfaces shown above, it is hard to control the wetting conditions as condensation

continues. In general, wetting transition [28-30] occurs while condensation goes on,

inducing the filmwise condensation, illustrated as Figure 1-5. Some scientists utilize

external energy to repel droplets, such as vibrating the condensing surfaces [31-34]

and electrostatic force to driving the droplet movement [35]. In contrast, using

internal energy is more crucial and practical in engineering application. Rough

microstructure modification is one of the solutions. It is investigated that the

4

condensing surface with hierarchical structures, as Figure 1-6, showing the

hydrophobic wettability can repel the droplets from the surface more easily and faster.

In Boreykos et al's study, carbon nanotubes were grown on silicon micropillars

resulting in the self-propelled jumping of condensates, as shown in Figure 1-7 [37].

Besides, Chen et al observed that the sizes of droplets decreased on two-tier textured

surface compared with smooth one by ESEM in Figure 1-8 [38]. From these aspects,

the hierarchical microstructure surface has ability to remove the droplets by itself and

minimize the condensate size. Also, the jumping phenomenon is relevant to heat

transfer performance.

With the coalescence of droplets, the jumping phenomenon occurs and resulting

in more regions to condense. This attracts researchers' attention to unsterdanding how

to trigger the jumping. So far, scientists find that the coalescence-induced jumping

phenomenon is relevant to surface structure, droplet size, and condensate properties

[39]. For the most common condition, microstructure has benefit for triggering

jumping and enhanced condensation heat transfer. In Figure 1-9, Miljkovic et al

utilized nanoscale copper oxide surfaces through CVD to achieve the efficient

jumping phenomenon and condensation heat improvement [6]. He also observed that,

with the rising in over-saturation of steam, or heat flux, condensing surface does not

allow to form micro-size droplets as lower heat flux; additionally, he considered it as

5

the consequence with the characteristic length and nucleation density, which implies

the much saturation, the less space for nucleation, and more difficult to trigger

jumping. In Yan et al's research, they investigated the droplet jumping dynamics on

nanostructured superhydrophobic, hierarchical superhydrophobic, and hierarchical

biphilic surfaces, respectively, by observing droplet velocity and jumping direction.

Besides, they made a diagram indicating the work of adhesion to the available surface

energy and contact angle as a function of droplet initial radii, as Figure 1-10 [39].

Accompanying the increase in supersaturation and heat flux, the jumping and

coalescence of droplets turns into flooding on condensing surface. Because of that,

scientists attempt to control the nucleation sites on surface and prevent the filmwise

condition [40, 41]. It is noted that the manipulation of surface morphology to change

the nucleating distribution affects the condensing process [42-47]. The patterns on

condensing surface could lead to complex wettability, motivating droplets into

combination and growing easily; finally, droplets escape from the surface and the

surface enter the next cycle of condensation. In Chatterjee et al's study, several

circular hydrophilic patterns with hydrophobic based regions are fabricated on copper

surfaces. By means of it, he successfully controlled the droplet distribution and

obtained the higher heat transfer coefficient with minimizing the circular pattern, as

shown in Figure 1-11 and 1-12 [42]. Peng et al made a hybrid surface composed of

interlaced hydrophobic and hydrophilic regions to conduct experiments. The results

they observed shown in Figure 1-13 [44] reveals that the heat transfer coefficient

would increase with the decrease in hydrophilic strip length, and generalized the

optimum of the width of hydrophobic region. On the other hands, the orientational

effects of the condensing surface is another factor to heat transfer. Lee et al from our

lab conducted experiments to compare between the horizontal and vertical surfaces, as

in Figure 1-14 [7]. He utilized spin coating to fabricate the copper surface, with

nanoscale silicon dioxide solution made by sol-gel method, into superhydrophobic

surface. Results indicated that the condensing surface is vertical, the heat transfer

coefficient increased with decreasing the strip width while for horizontal downward

surface showed the converse phenomenon, as in Figure 1-15.
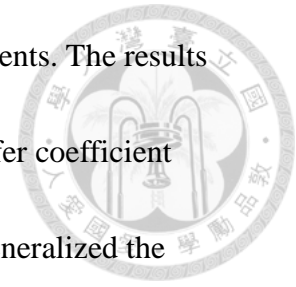
1.2.2 Carbon Nanotube (CNT)
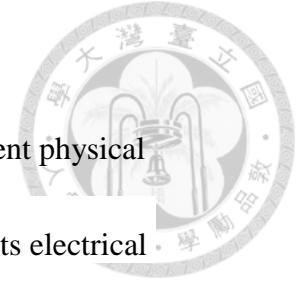
Carbon nanotube attracts attention in this decade for its excellent physical properties and applications. To most applications, CNT is used for its electrical conductivity. In semiconductivity industries, Pacchini et al studied the CNT printed paper with Ag layer to explore the electromagnetic effect on the resonant circuits [48]. Also, several researchers utilized screen printing to print CNT onto substrates as electronic networks [49-51]. On the other hands, thermal enhancement [52, 53] and optical properties are also investigated. Marconnet et al conducted experiments to enhance the thermal conductivity by electroplating CNT films [52]. They concluded that the thermal conductivity after electrodeposition was nearly 3 W/m/K, which is comparatively high for such low density films, as FIgure 1-16. Bera et al utilized simple spraying coating to fabricate the CNT/AlOOH coating, and investigated the absorptance under different temperature and time, as Figure 1-17 [54]. From these studies, it is noted that fabrication methods of CNT are relevant to the applications. As for researches relating condensation, wettability of modified surface is often considered as the approach.

As for the coating of CNT, wettability is mostly measured as hydrophobicity [55-57]. Journet et al measured the contact angle of droplet on nanotube forest, and the results showed superhydrophobic wettability [55]. In 2014, Aria et al studied

8

droplet impact dynamics of superhydrophobic CNT arrays [56]. They fabricated the

surface by vacuum annealing treatment and found the surface had well ability to repel

water droplets, as Figure 1-18. Besides, in order to fabricate on metallic surface, heat

treatment [53,54, 56] or chemical vapor deposition [58-59] are accompanied by the

procedures. But for experimental process, using simple ways to fabricate CNT films

or layers is still worth discussing.
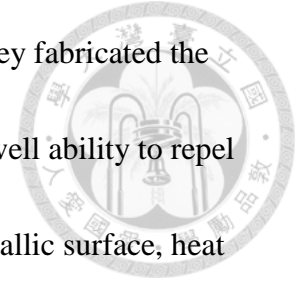
1.3 Purpose

From the researches above, it is potential to consider hybrid materials into

fabricating coating on condensation heat transfer. Also, effects of simple methods

used for CNT coating are rarely discussed. Combining the two factors, in this research,

I investigated the effects of different area ratio of CNT film, which was fabricated by

rolling printing, and observed the wetting conditions of the condensing surfaces under

a close chamber with steam-air mixture. And finally, studied the condensation heat

transfer from it.

9
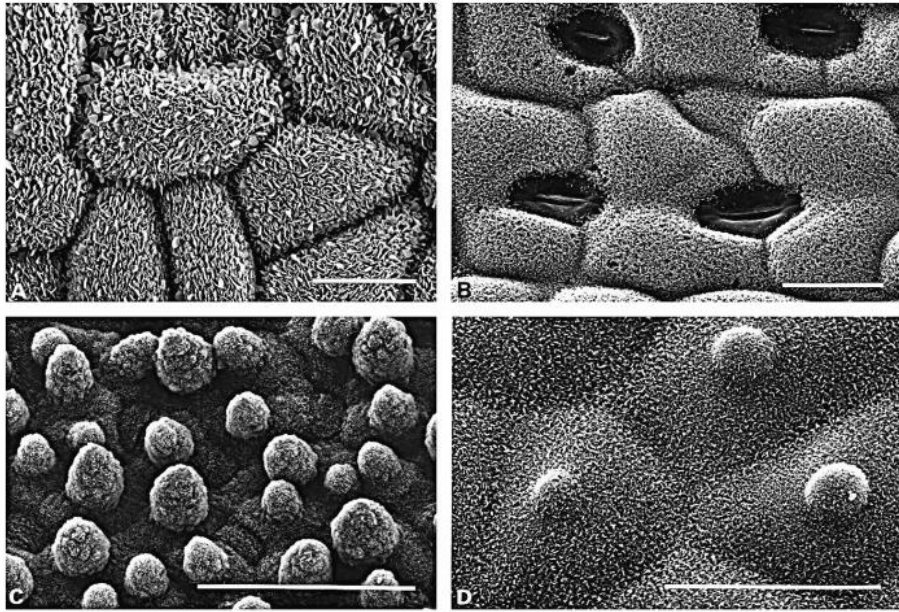
Figure 1- 1. Lotus surface on leaves. [14]
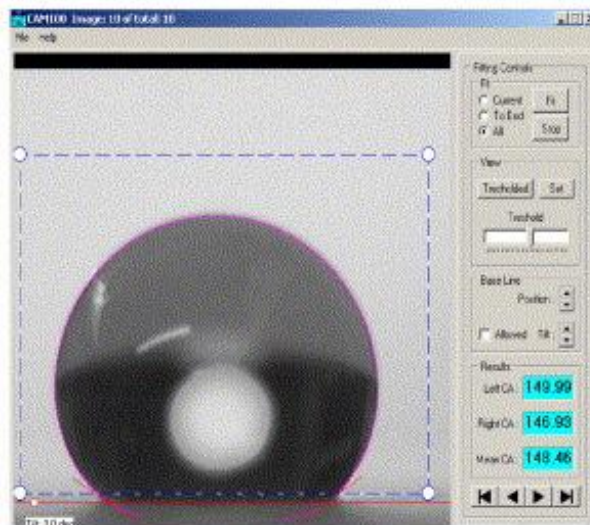
Figure 1- 2. Contact angle measurement for *n*-octadecyl mercaptan on the surface
before experimentation. [24]

10
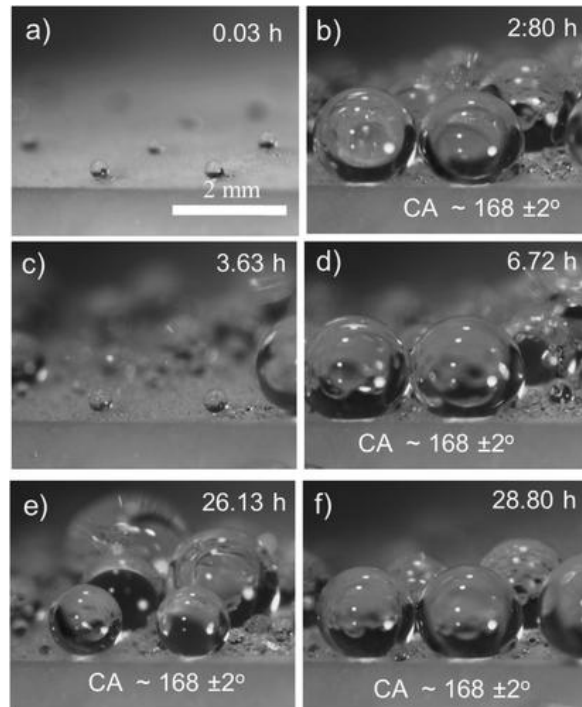
Figure 1- 3. Optical microscope images during condensation. [26]
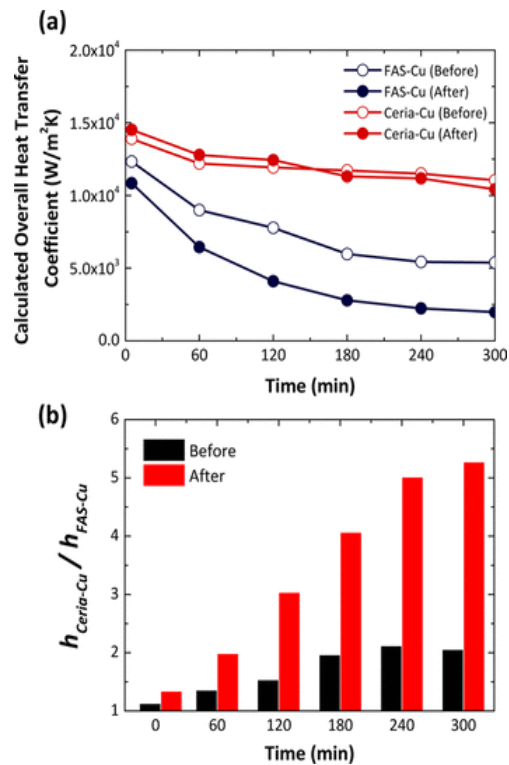
Figure 1- 4. Calculated overall heat-transfer coefficient of each sample, and the
comparison between ceria-Cu and FAS-Cu. [27]

11
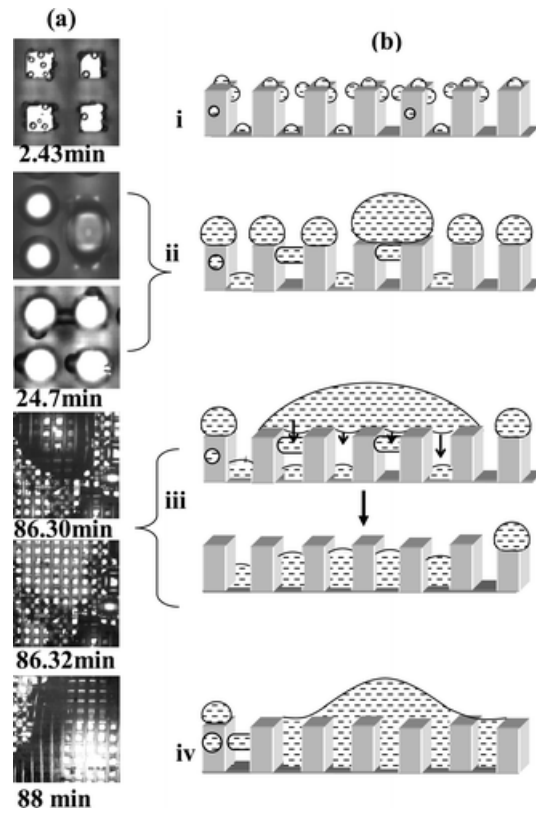
Figure 1- 5. The illustration of wetting transition. [28]
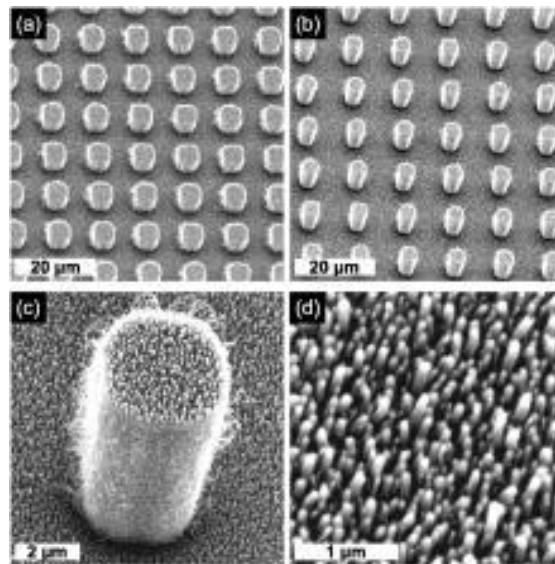
Figure 1- 6. Hierarchical structure surface. [36]
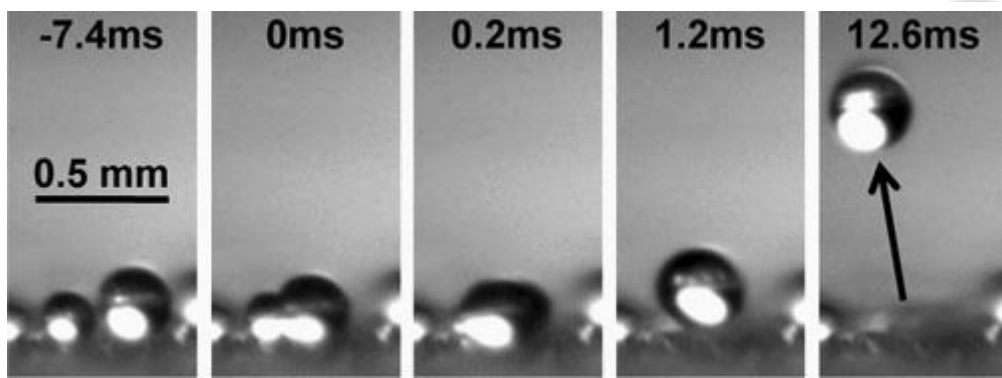
Figure 1- 7. Self-propelled jumping of condensates. [37]
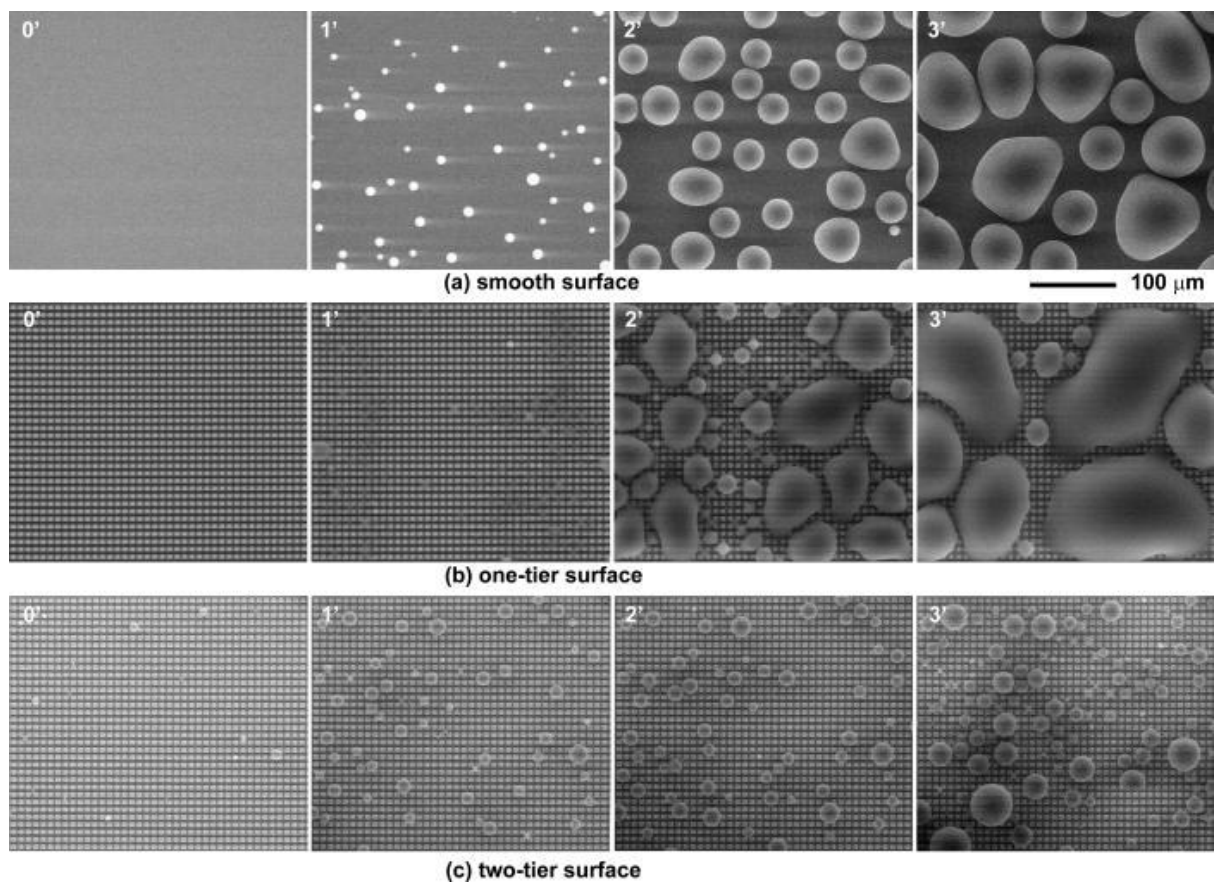
Figure 1- 8. Water vapor condensation on fluoropolymer-coated silicon surfaces in ESEM. [38]

13
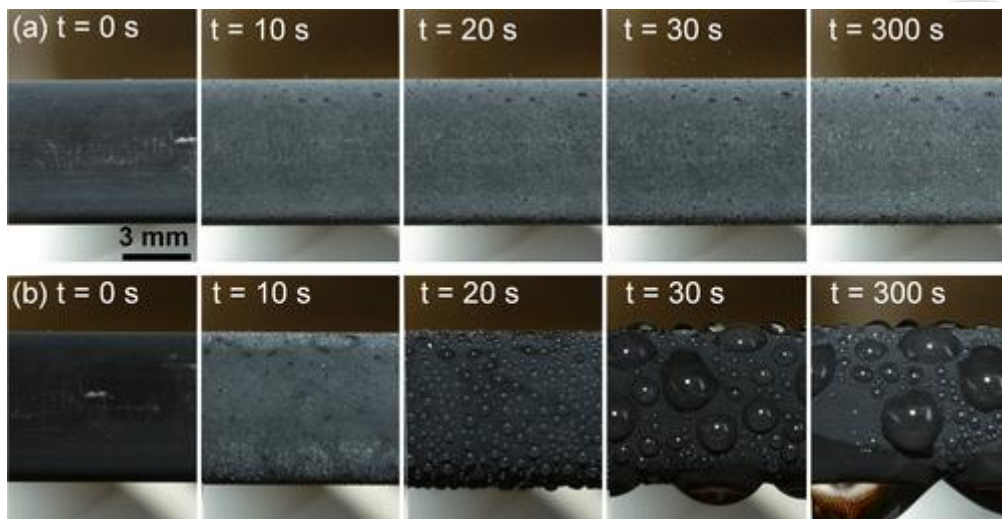
Figure 1- 9. Jumping and flooded condensation. [6]
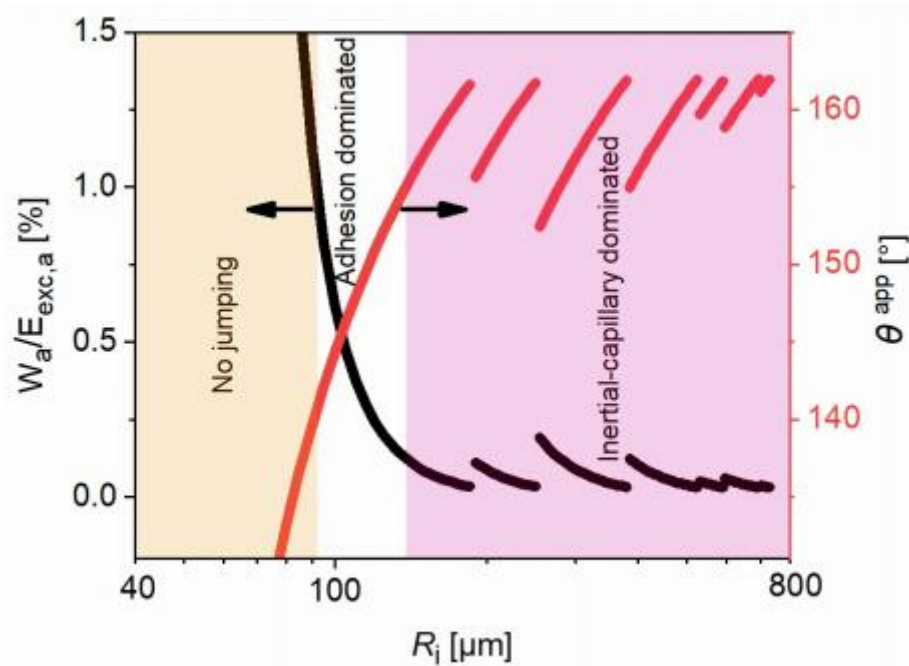
Figure 1- 10. Ratio of work of adhesion to the available excess surface energy $W_a/E_{exc,a}$ and droplet apparent contact angle θ_{app} as a function of droplet radius R_i on the hierarchical biphilic surface. [39, S7]

14
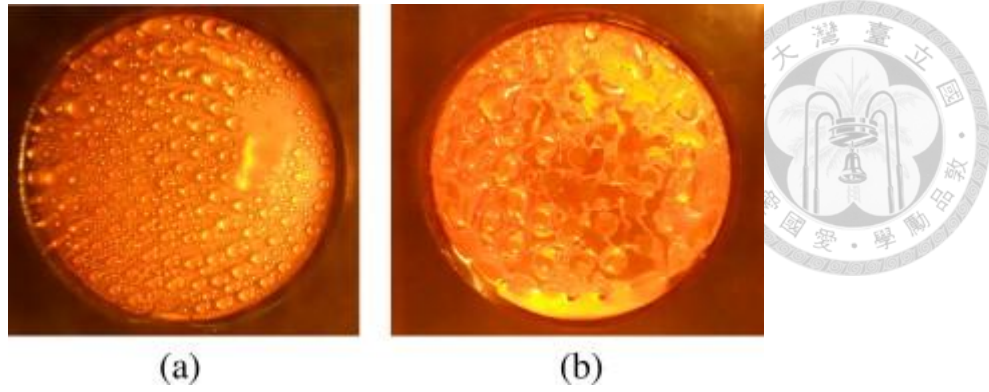
Figure 1- 11. Comparison of droplet distribution between two different circular

pattern types. [42]
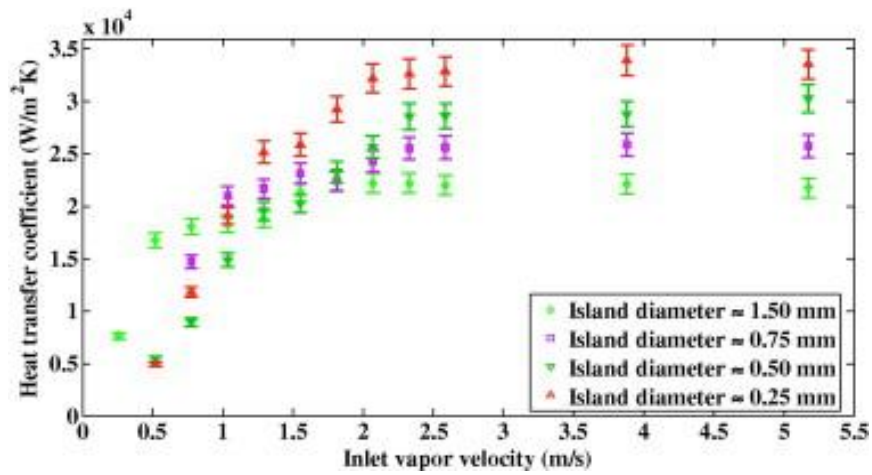
Figure 1- 12. The highest heat transfer coefficients observed for the patterned

condensation surface with various hydrophilic island diameters. [42]

15
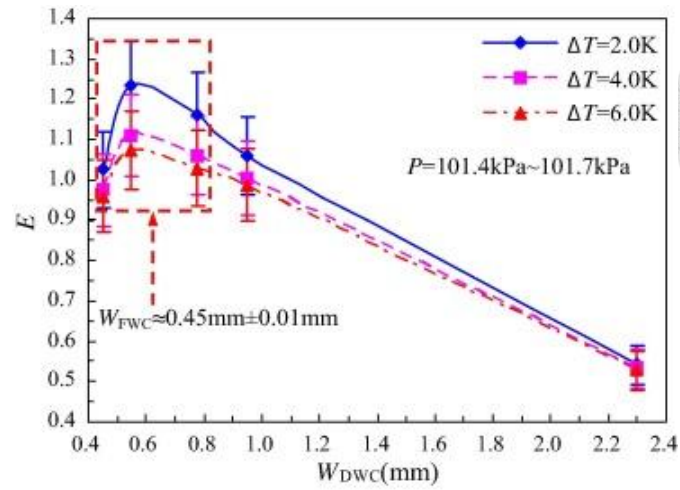
Figure 1- 13. Influence of hydrophobic region width on heat transfer enhancement
factor of hybrid surface at different surface subcoolings. [44]
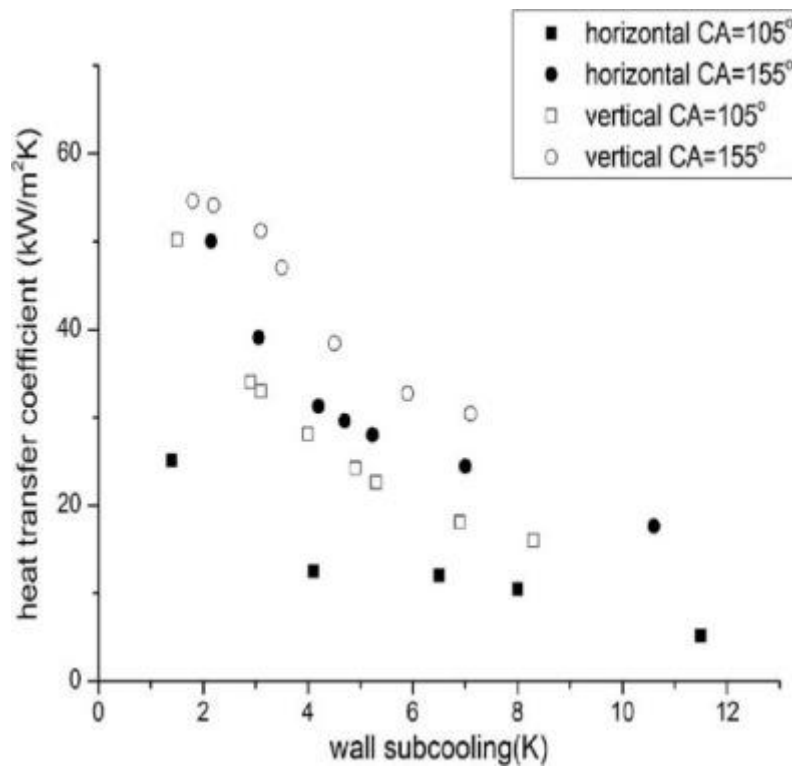
Figure 1- 14. Variation of heat transfer coefficient with wall subcooling for plain and
superhydrophobic surfaces. [7]

16
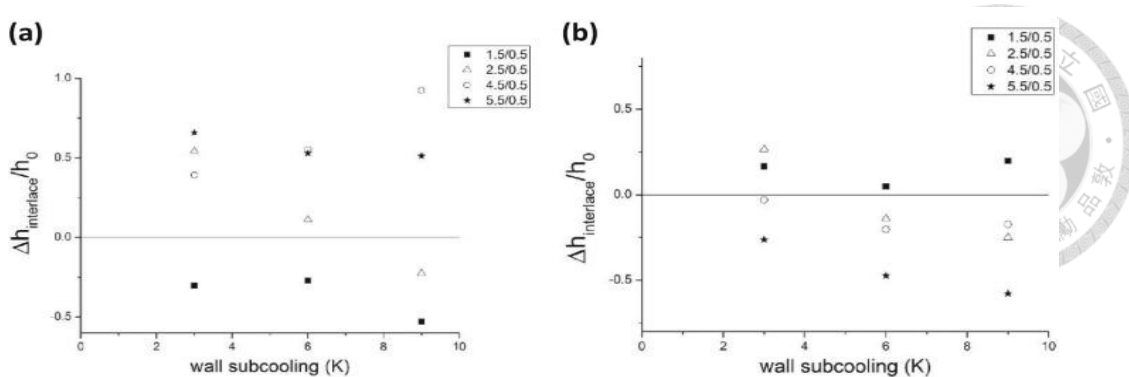
Figure 1- 15. Additional heat transfer enhancement ratio of various types of modified surface as a function of wall subcooling for the (a) horizontal and (b) vertical surfaces. [7]
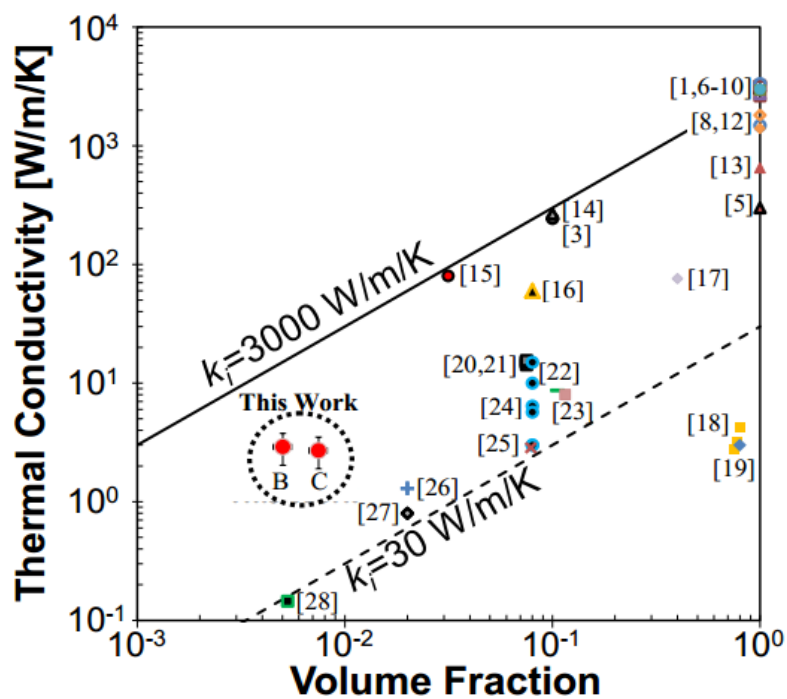
Figure 1- 16. Thermal conductivity as a function of volume fraction for CNT films compared to values reported for measurements for vertically-aligned CNT arrays and individual nanotubes (volume fraction = 1). [52]

17
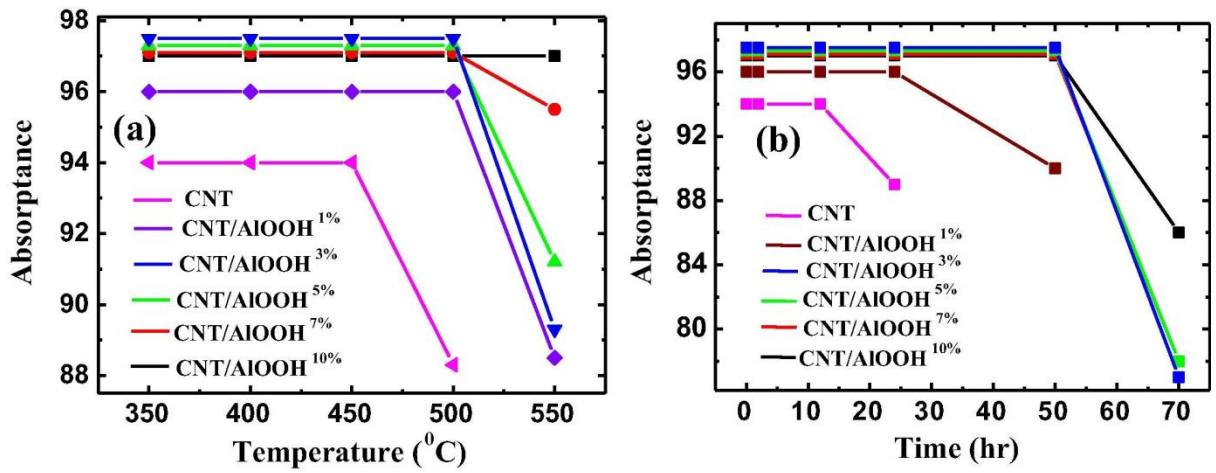
Figure 1- 17. Absorptance of CNT and CNT/AlOOH coatings. [54]
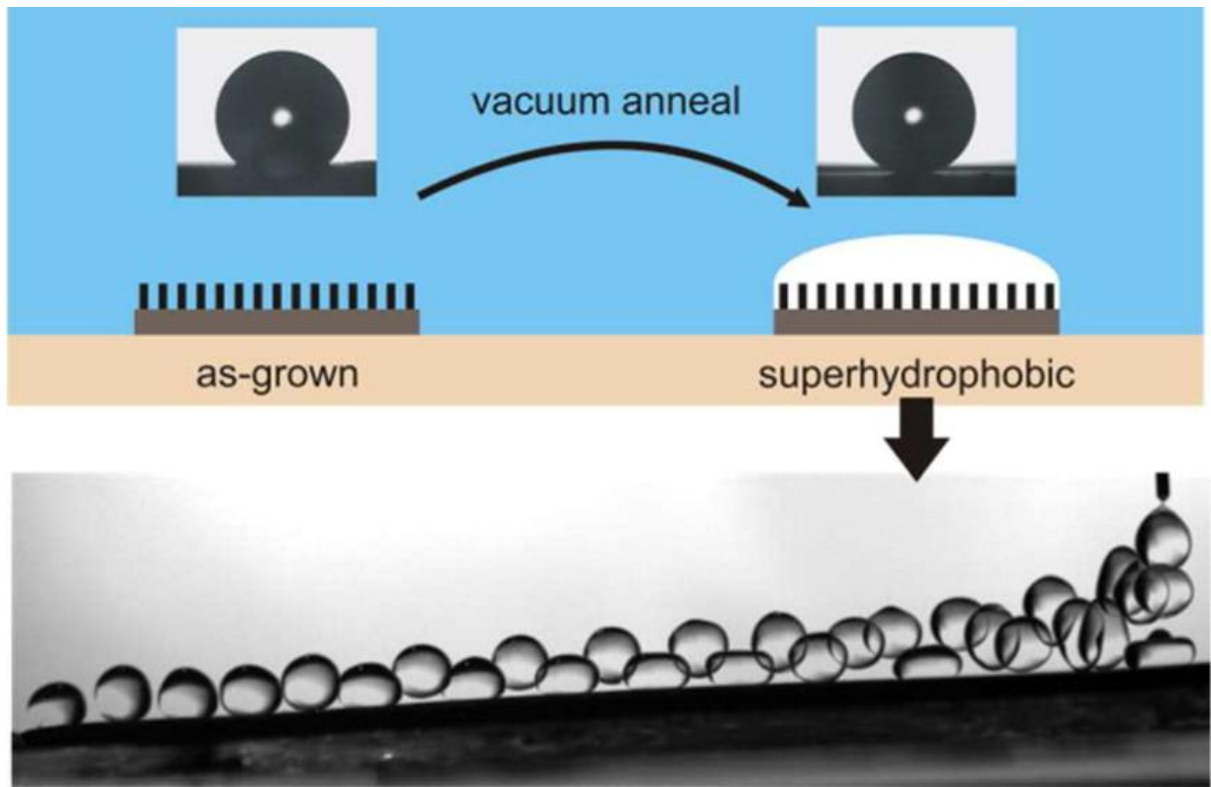
Figure 1- 18. The illustration of microsturcture and droplet movement. [56]

Chapter 2. Theory

2.1 Surface Wettability

2.1.1 Wettability and Contact Angle Theory

Surface wettability is a characteristic related to the gas, liquid, and solid when

wetting phenomenon happens. Besides, the physical mechanism of wetting can be

interpreted by tensions between contacting materials; in other words, $\gamma_{LG}, \gamma_{SG}, \gamma_{SL}$ are

the surface tensions of liquid and gas, solid and gas, and solid and liquid, respectively.

More clearly, the wetting phenomenon consists of three types according to the balance

of liquid on surface: adhesion, immersion, spreading, as Equation 2.1, 2.2, 2.3,

respectively. [60]

$$\gamma_{LG} + \gamma_{SG} - \gamma_{SL} > 0 \tag{2.1}$$

$$\gamma_{SG} - \gamma_{SL} > 0 \tag{2.2}$$

$$\gamma_{SG} - \gamma_{SL} - \gamma_{LG} > 0 \tag{2.3}$$

While the liquid is equilibrium, the state of it contacting a solid surface with air

around can be illustrated in Figure 2-1; by force balance in Newton's law, the

following equations are used to describe this equilibrium.

19

$$\gamma_{LG} + \gamma_{SG}\cos\theta + \gamma_{SL}\cos\alpha = 0 \tag{2.4}$$

$$\gamma_{LG}\cos\theta + \gamma_{SL} + \gamma_{SG}\cos\beta = 0 \tag{2.5}$$

$$\gamma_{LG}\cos\alpha + \gamma_{SL}\cos\beta + \gamma_{SG} = 0 \tag{2.6}$$

$$\alpha + \beta + \theta = 2\pi \tag{2.7}$$

$$\gamma_{ik} + \gamma_{kj} > \gamma_{ij} \tag{2.8}$$

α, β, θ are angles between three tensions. It is noted that Equation 2.8 means the constraint by force balance. The contact angle "θ" can be defined as $\beta = \pi$, indicating the wetting happens upon a flat surface plane. Moreover, when $180°>\theta>90°$, the surface has hydrophobic characteristic; in contrast, when $\theta<90°$, the surface belongs to hydrophilic property. Other definition of superhydrophobic and superhydrophilic characteristics are shown in Table 2-1.

2.1.2 Young's Equation

Young's equation considers a situation that droplet stays on flat, smooth, and homogeneous plane without gravitation effect. This model represents an equilibrium state between surface tensions, such as shown in Figure 2-2 and Equation 2.9. γ_{SG}, γ_{SL}, and γ_{LG} are interfacial tensions between solid and vapor, solid and liquid, and liquid and vapor, respectively where theta is the contact angle. In spite of this perfect illustration, it is inappropriate to apply it on most engineering and industry due to the

20

surface roughness and the complex micro/nano structure. With such consideration,

Wenzel proposed a theory enabling to describe real wetting model [61].

$$cos\,\theta = \frac{\gamma_{SG} - \gamma_{SL}}{\gamma_{LG}} \tag{2.9}$$

2.1.3 Wenzel Model

Wenzel model is illustrated in Figure 2-3, which considers rough structure on the

surface. He assumed that the liquid on the surface occupies the tiny gaps and so that

completely wets the surface; in other words, the edges becomes only solid-liquid

interface. Under this hypothesis, the contact can be obtained as following equation:

$$cos\,\theta_{We} = R\,cos\,\theta \tag{2.10}$$

θ_{We} is the contact angle of rough surface; θ is the contact angle of smooth surface

with the same substrate material. R means toughness ratio, defined as the ratio of

actual contact area to the projected area on substrate surface. Based on Wenzel model,

superhydrophobic and superhydrophilic surface can be fabricated via producing

nano/ micro scale structure on hydrophobic and hydrophilic surface, respectively.

However, Wenzel model cannot apply under extreme situation such as large contact

angle and roughness, supported by Lafuma in 2003 [62]. As for such condition, Cassie

and Baxter proposed another wetting model [63].

21
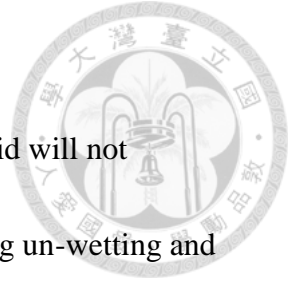
2.1.4 Cassie-Baxter Model

Compared with in Wenzel model, in Cassis-Baxter model, liquid will not

penetrate into the gap but stay on the top structure of surface, leaving un-wetting and

air-contacting regions inside the structure. The illustration shows in Figure 2-4;

furthermore, the complex interface between air, liquid, and solid surface can be

deduce into Equation 2.11 to describe. θ_{CB} is the contact angle for Cassie-Baxter

model, while θ is the smooth contact angle under the same substrate surface and φ_S

is the area fraction of liquid onto solid surface.

$$cos\,\theta_{CB} = \varphi_S(cos\,\theta + 1) - 1 \qquad (2.11)$$

2.1.5 Partial Wetting Model and Wetting Transition

Whether as for Wenzel model or Cassie-Baxter model, it is crucial to consider

the surface roughness and intrinsic contact angle to describe the wetting phenomenon.

Cassie-Baxter model is easier for droplet repelling due to the less contacting area

leading to lower surface energy barrier between liquid and solid to overcover. In

addition, Miljkovic observed the partial wetting model [64], as Figure 2-5. They

concluded that the partial wetting model between Wenzel and Cassie-Baxter model

has better heat transfer performance. On the other hands, wetting transition is also an

approach to to discuss.

Wetting transition occurs when Cassie-Baxter Model turns into Wenzel Model. It

22

is related to energy barrier between droplet and contacting surface. Bormashenko

concluded the energy barrier between these two model is as following [65]:

$$W_{tr} = 2\pi a^2 \frac{H}{l}(\gamma_{SL} - \gamma_{SG}) = -2\pi a^2 \frac{H}{l}\cos\theta \qquad (2.12)$$

Besides, the growth of droplets depends on the pressure. As growth reaches a level,

edges of droplet would changes, which indicates the transition happens. Zheng

concluded the critical pressure for the transition, as the following relation [66]:

$$p_c > -\frac{\gamma\varphi_S \cos\theta}{(1-\varphi_S)\lambda} \qquad (2.13)$$

Whether controlling microstructure or using external force to stabilize that

droplets stay on surface, wetting transition occurs while growth and coalescence

continues. It is noted that wetting model turns from dropwise into filmwise wettability

as nucleation density rises. As a result, wetting model affects the condensation heat

transfer.

23
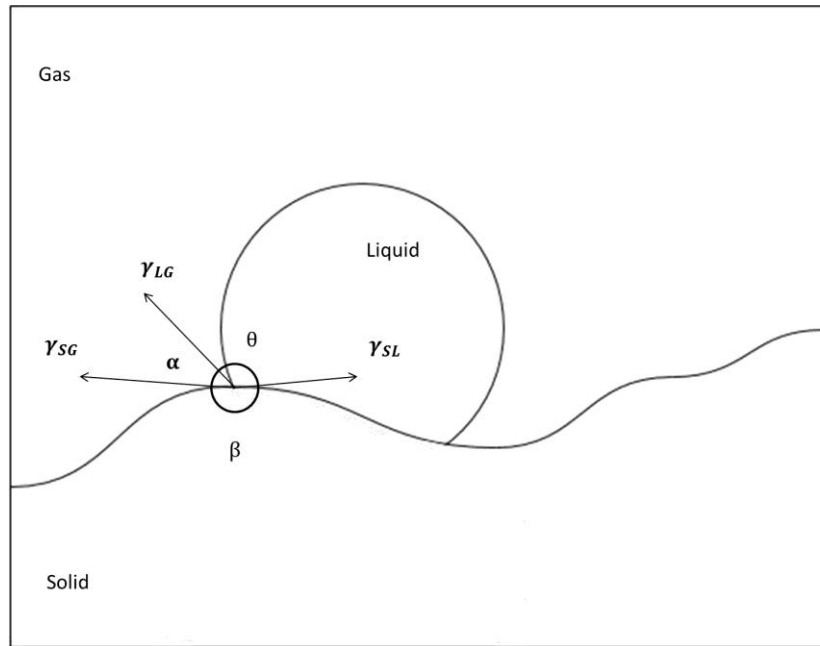
Figure 2- 1. Force balance of droplet on a surface.
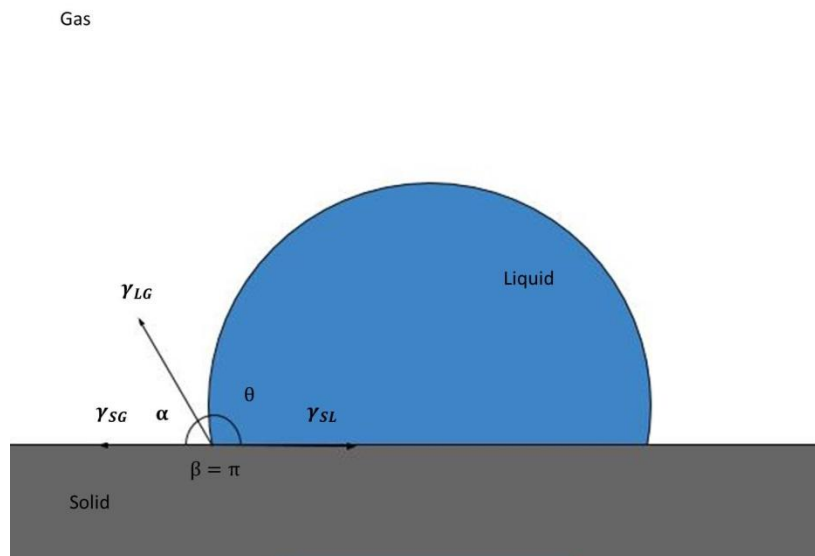
Figure 2- 2. Illustration of Young's Equation.

24
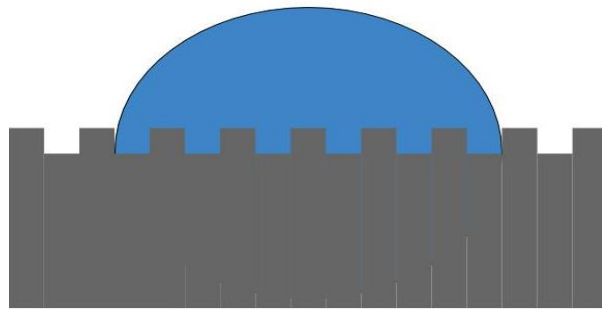
Figure 2- 3. Wenzel Model.
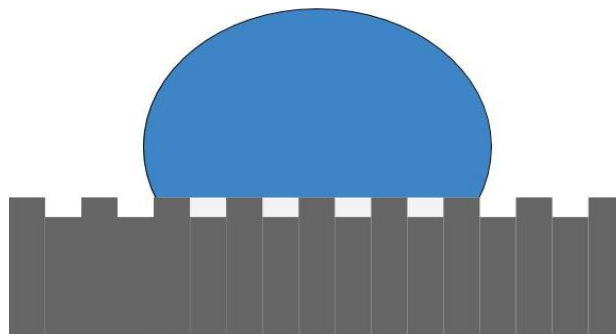
Figure 2- 4. Cassie-Baxter Model
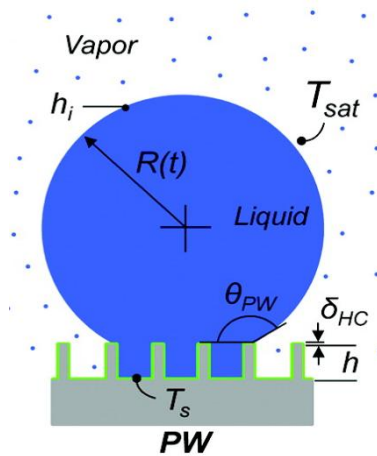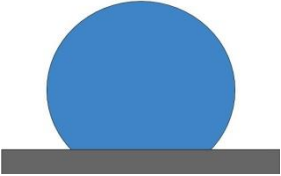
Figure 2- 5. Partial wetting model. [64]

25

Table 2- 1. Various types of wettability.

Wettability	Droplet situation
superhydrophilic ($\theta < 10°$)	
hydrophilic ($90° > \theta > 10°$)	
hydrophobic ($150° > \theta > 10°$)	
superhydrophobic ($\theta > 180°$)	

26

2.2 Condensation Heat Transfer

2.2.1 Stages of Condensation

One cycle of condensation heat transfer can be separated into three stages:

nucleation, growth and coalescence, and removal. The following parts include the

discussion of three stages and effects of subcooling degrees.

2.2.1.1 Heterogeneous Nucleation

Heterogeneous nucleation comes from energy absorption which leads to the form

of cluster, and induces the phase change. Classical nucleation theory indicates that an

energy barrier is overcome; as following, the nuclei formation happens. The energy

barrier equation is shown as following:

$$\Delta G = \frac{4}{3} r_e^2 \gamma_{lv} \frac{2 - 3\cos\theta + \cos^3\theta}{4} \qquad (2.\,14)$$

r_e is the equilibrium and minimum radius for the nuclei, in order to further condensate

and grow the droplets. r_e can be determined by the following [67]:

$$r_e = \frac{2 v_l \gamma_{lv} T_W}{h_{lv}(T_{sat} - T_w)} \qquad (2.\,15)$$

Besides, the nucleation rate can be obtained by:

$$J = J_0 e^{(-\Delta G / k_b T)} \qquad (2.\,16)$$

J_0 is the nucleation constant, which depends on the material, k_b is Boltzmann constant,

and T is the surface temperature. Equation 2.16 reveals that the effect of difference in

energy barrier is dramatic because of the exponential relation in the equation; in addition, the wettability affects the energy barrier. Also, the wall temperature is another factor. As the wall temperature increases, meaning the wall subcooling temperature decreasing, the nucleation rate declines, and vice versa.
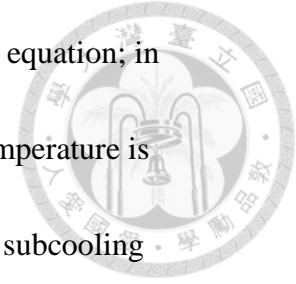
2.2.1.2 Growth and Coalescence

After the nucleation, the nuclei start to turn into droplets, and follows the two stages to condensate: growth and coalescence. The first stage results from the cluster of molecules nearby, which occurs after the nucleation immediately. Besides, with the higher surface area of the nuclei, the the higher the growth rate is. The second stage happens as the size is big enough for the contact between droplets nearby, adjacent droplets combining, and then droplet continues growing up. In 1995, Beysens pointed out the relation between radius of droplet and time as following [68]:

$$r \propto t^{\eta} \tag{2.17}$$

The regime of droplet growth is precisely different in the first and second stages, which induces that the η is distinct. Figure 2-6 shows that the mean droplet radius change with time deduces the distinct value η corresponding to growth and coalescence stages [28]. At the first stage, the volume of the droplet is proportional to the time with $\eta= 1/3$; after entering the coalescence, η becomes 1/2, with higher rate of droplet growth. At last, the droplet would repel from the condensing surface until

28
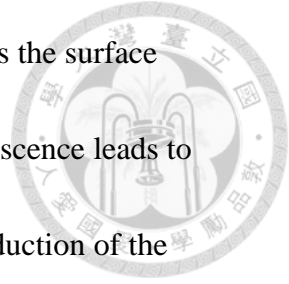
the gravitational or external force applying on the droplet overcomes the surface

tension. From these mechanism, the more rapid of growth and coalescence leads to

the more efficient condensation heat transfer; in other words, the reduction of the

duration in condensing cycle is better.

<u>2.2.1.3 Removal</u>

From the description of the last paragraph, the removal occurs in the end of he

condensing cycle. In general, gravity is the external force applying on the droplet; in

addition, gravity increases with the growth of the droplet. The force can be obtained

from the following equations [69]:

$$F_{ga} = \frac{1}{3}\rho g\pi r^3 (2 - 3\cos\theta + \cos^3\theta)\sin\alpha \qquad (2.18)$$

$$F_{gn} = \frac{1}{3}\rho g\pi r^3 (2 - 3\cos\theta + \cos^3\theta)\cos\alpha\sin\phi \qquad (2.19)$$

F_{ga} and F_{gn} are gravitational force along with and perpendicular to the axial

direction, respectively, where ρ is the density of droplet, g is the gravitational

acceleration, r is the radius of droplet, θ is the contact angle, α is the inclined angle of

tube, and ϕ is the azimuthal angle. The external forces, related to the angles defined

as above, applied on the tube are shown as Figure 2-7 [69].

Besides, the viscous force on the droplet can be determined as following [69]:

$$F_\sigma = 2\sigma r \sin\theta (\cos\theta_{rec} - \cos\theta_{adv}) \qquad (2.20)$$

σ is the surface tension of the droplet, where θ_{rec} and θ_{adv} are receding and

29

advancing angle of the droplet.

Based on the Equation 2.19 and 2.20, the repelling radius of droplet on the tube

can be determined as following:

$$r_{max} = \left[\frac{6\sigma \sin\theta(\cos\theta_{rec}-\cos\theta_{adv})}{\rho g\pi(2-3\cos\theta+\cos^3\theta)\sin\theta}\right]^{0.5}$$
(2. 21)

While Ø is 0 ° and 180 °, Equation 2.21 becomes:

$$r_{max} = \left[\frac{6\sigma \sin\theta}{\rho g(2-3\cos\theta+\cos^3\theta)}\right]^{0.5}$$
(2. 22)

which corresponds to our experimental situation.
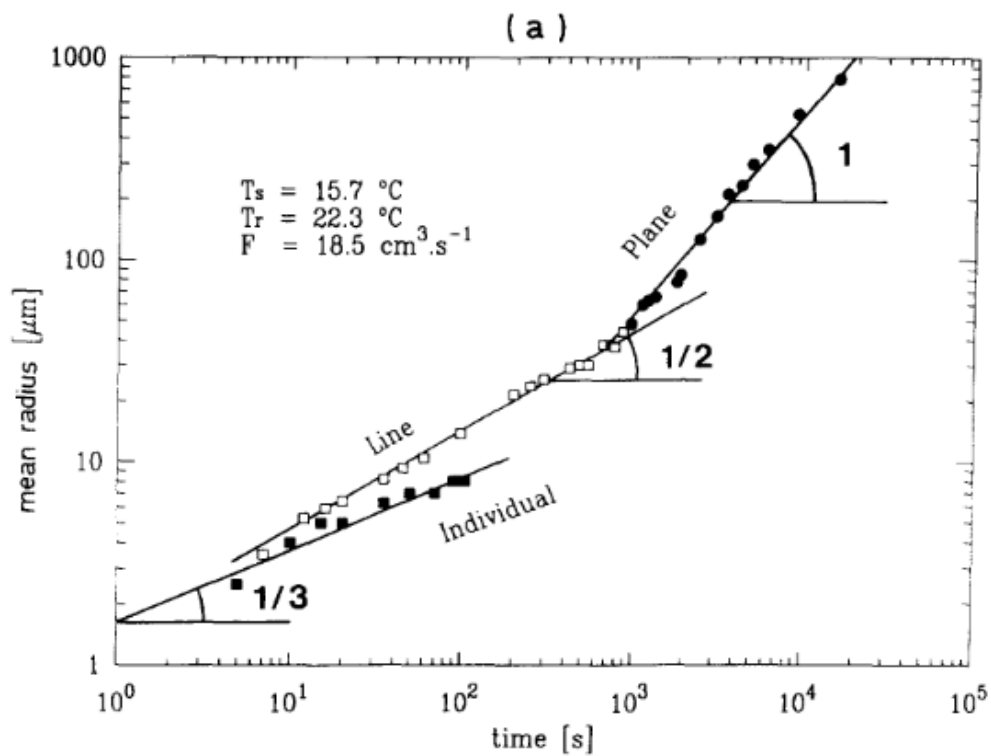
Figure 2- 6. The mean droplet radius grows with time for different growth and

30

coalescence stages. [28]
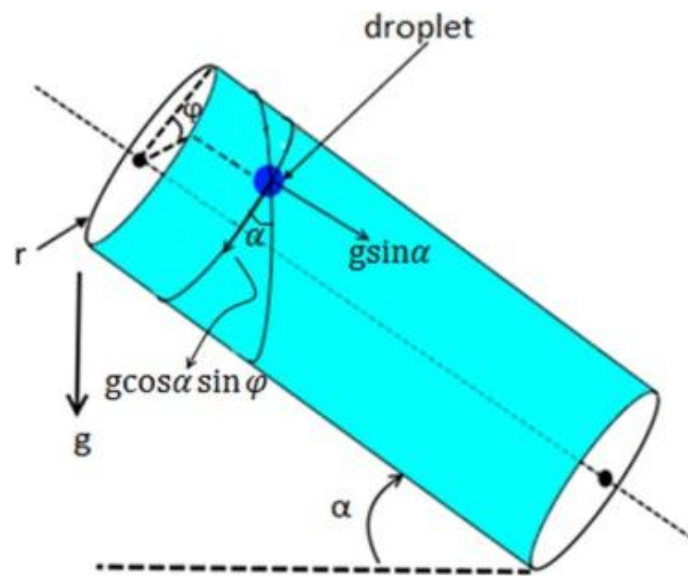
Figure 2- 7. The external forces applied on the tube. [69]

2.2.2 Effects from Non-condensable Gas (NCG)
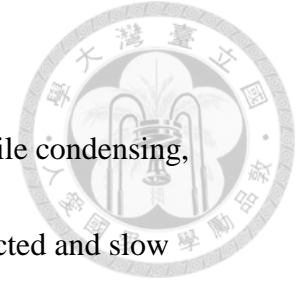
Non-condensable gas play another factor to condensation. While condensing, droplets form and emerge upon the surface, which would be obstructed and slow down by the boundary layer from non-condensable gas. Moreover, this phenomenon happens as surface subcooling degree increases, inducing the less efficient heat transfer. The diffusion mechanism of gas inside the condensing environment is simulated by the vapor pressure, or the saturation pressure. As NCGs flow into the regions between the the atmosphere and the surface, gas boundary layer forms and causes the impediment in condensation, which illustrated as Figure 2-8. Also, heat resistance from the boundary layer affects the heat transfer.

Ma et al found that the 1% increase in the concentration of NCGs leads to the decrease in heat flux [70]. However, they observed the coalescence and removal of droplets disturbs the boundary layer. Besides, Wen et al studied the effect of enhancement in condensation from this disturbance [71]. They used the hydrophilic surface with hydrophobic bumps to trigger the falling droplets, disturb the NCG boundary layer, and increase water vapor diffusion, as Figure 2-9.

To sum up, the dropwise condensation has better performance than the filmwise one when NCGs exist. In addition, various materials used as coating on substrate surface is worthy of investigating the coalescence and removal of the droplets, in

other words, the condensation heat transfer resulting from hybrid coated surface.
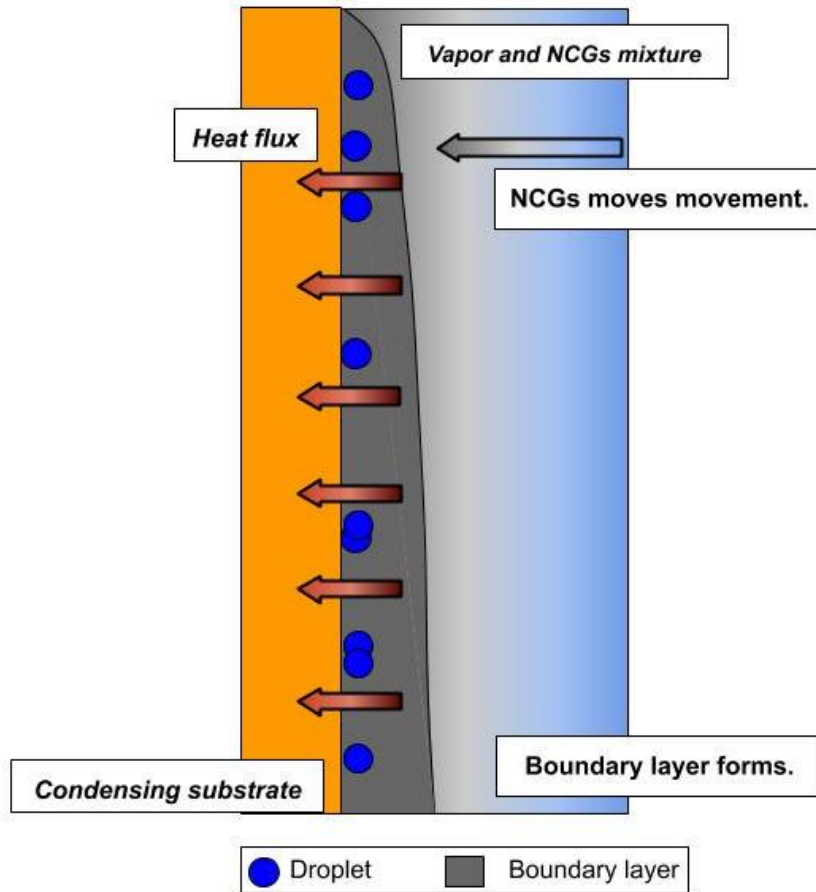
Figure 2- 8. The Illustration of NCGs boundary layer.
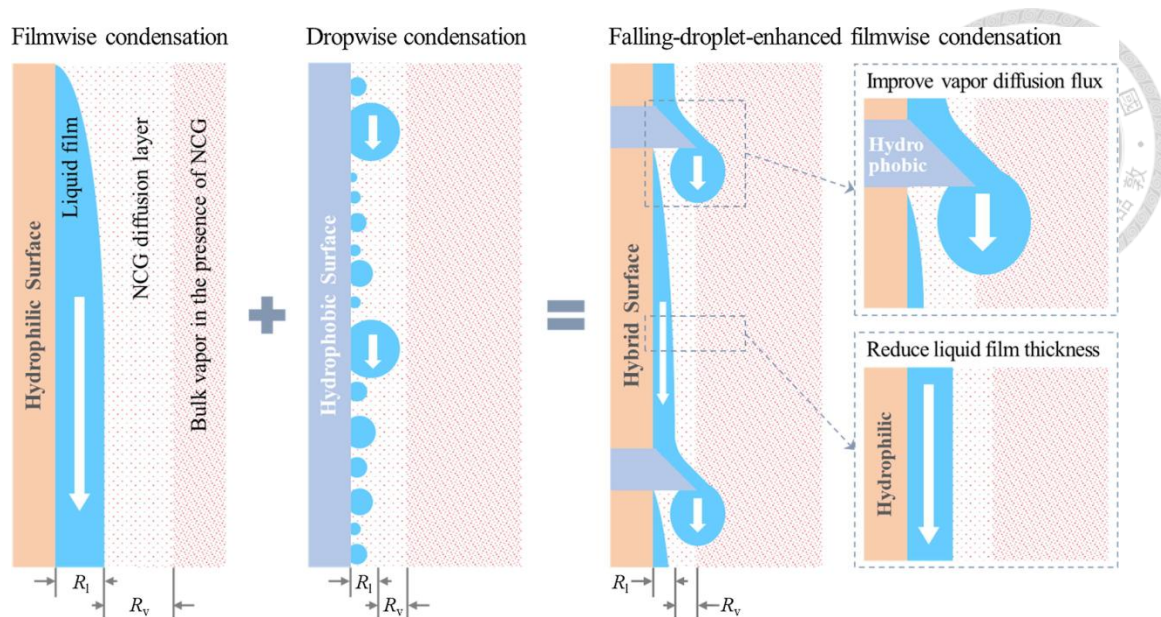
Figure 2- 9. Hydrophilic surface with hydrophobic bumps to enhance the droplet falling. [71]

Chapter 3. Experiments

3.1 Surface Modification

3.1.1 Chemical and Materials

1. Deionized water

2. MWCNT---AC tube-030(>98%）

   From: Golden Innovation Business co.,Ltd.

3. Methanol (99.9%）

   From: ECHO Chmical co. Ltd.

4. Hardener---NS150

   From: Photo.cure co., Ltd

5. Acetone (99.9%）

   From: UNI-ONWARD Corp.

3.1.2 Equipment

To prepare the CNT ink

1. Ultrasonic cleaner---Bransonic 3510

   From: Barsonic

2. Electronic scale---GX400

   From: A&D co., Ltd.

3. Beaker & Dropper

To prepare and polish the copper surface

1. Sandpaper #800, #1000, #1200, #2000

2. Acetone safety wash bottle

From: Chuan Chi Trading co., Ltd.

To conduct the surface modification

1.   Furnance---Hong Sen HS-101

From: Chung Chuan

2.   Tape mask

3.   Holder

From: NTU Mechanical Workshop

To measure the parapeters

1.   Contact Angle Goniometer---Model100SB

From: Sindatek
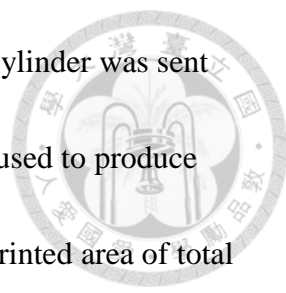
2.   Electronic scale---GX400

From: A&D co., Ltd.

3.1.3 Procedures

Surface preparation

Firstly, the copper surface is polished with sand papers from #800 to #2000 in

order to remove the oxidation and chemicals from the surface. Deionized water and

36

acetone are used to wash the polished surface, and then the copper cylinder was sent

into the furnace for drying. After cleaning the surface, tape mask is used to produce

the different types of modification. In this study, to investigate the printed area of total

condensing surface is the main factor, which is to compare the effect of 0% (plain

copper), 30%, 50%, 70%, and 100% (all printed copper). The total length of

condensing area is 30cm; thereby, the corresponding printing length (m) of 30%, 50%,

70% types are 10cm, 17cm, and 20cm, which is illustrated as Figure 3-1 and Table

3-1. The wider the printing length (m) is, the smaller the plain area is. Besides, the

contact angle (CA) and the printed weight were measured and listed as Table 3-1. The

100% printed cylinder is shown in Figure 3-2.

As for the parameters measured, the first one to be discussed is the contact angle

(CA), which is measured with contact angle goniometer. Initially, normal copper

surface is hydrophilic with CA around 75°. However, for plain area after cleaning, the

wettability is hydrophobic with CA around 107 °, while the printed area is relative

hydrophilic with CA around 76 °. It is noted that the surface roughness of printed area

is nonuniform in microscale due to the printing procedure; as a result, the printed

weight were recorded by electronic scale in order to make sure the ink printed on the

copper surface is reasonable corresponding to area ratios. The next step is to prepare

the ink and printing.

37
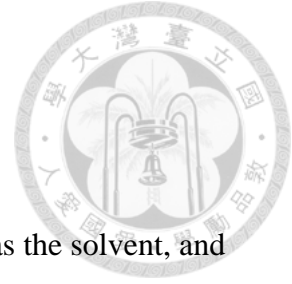
Ink preparation and cylinder printing

The ink is composed of MWCNT, as the solute, the hardener, as the solvent, and methanol, as the dispersion. To begin, add MWCNT into the hardener to prepare the viscous solution with the proportion 1 gram: 0.1 gram. Then use the ultrasonic cleaner as Figure 3-2 to degas the solution. After stirring and degas add methanol into the solution with proportion 1.1g of solution: 0.5 milliliter of methanol. Then use the ultrasonic cleaner to degas again. After degased and stirring, the ink is prepared to print the copper cylinder.

Before printing, I designed a holder to make sure the polishing and printing is under stable circumstance. The design is shown in Figure 3-3 made of bearings and aluminium alloy plates. The prepared ink was put on a rectangle plate; then, this plate was set below the held cylinder and between the holder walls. Pushing the inked plate to rolling print the cylinder surface ink, the cylinder surface would be covered with the ink. After printing, the cylinder was sent into furnace for 30 minutes to dry the ink. At last, the printed was prepared to conduct the experiments.

Partial coated copper

30% printeded copper

l　*m*　*l*

Pure copper

50% printeded copper

100% printed copper

70% printeded copper
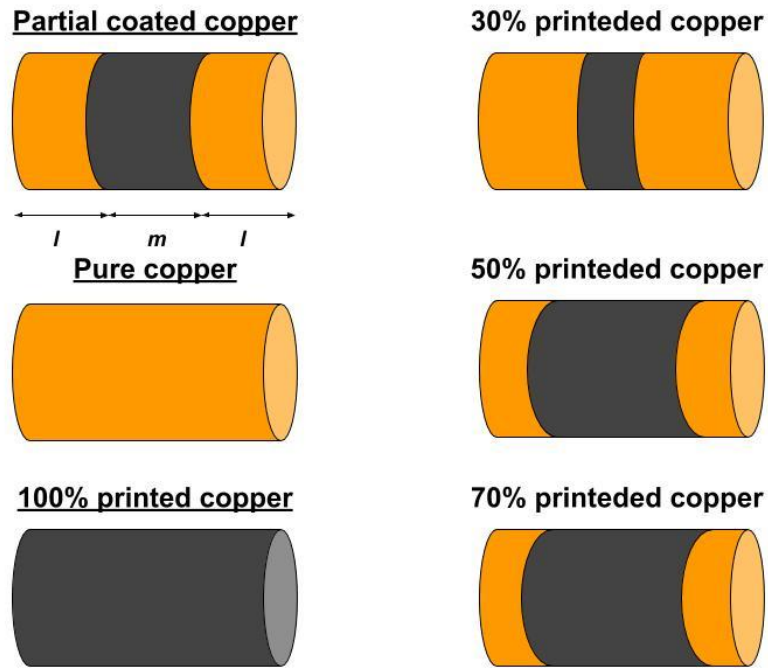
Figure 3- 1. Illustration of different types of printed area ratio on cylinder surface.

Table 3- 1. List of the surface types and corresponding parameters.

Types	Printing length (*m*)	Half Plain length (*l*)	CNT ink weight	CA of CNT printed area	CA of plain copper
0% (Plain)	0 mm	30 mm	0 g	~76 °	Before cleaning:75 °
30% Printed	9 mm	10.5 mm	0.12 g		
50% Printed	15 mm	7.5 mm	0.215 g		After cleaning: ~107 °
70% Printed	21 mm	4.5 mm	0.428 g		
100% Printed	30 mm	0 mm	0.586 g		

Figure 3- 2. The 100% printed cylinder.

Figure 3- 3. The ultrasonic cleaner.
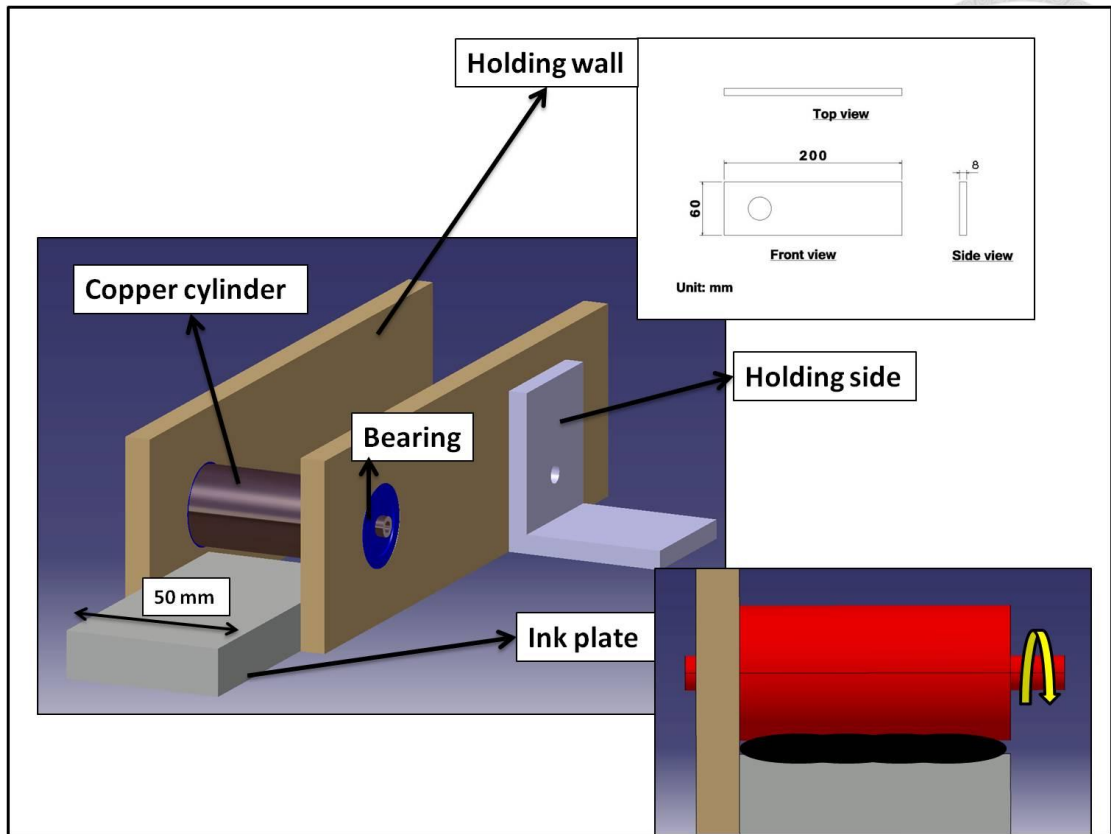
Figure 3- 4. The design of holder.

3.2 Thermal System

3.2.1 Equipment

1. Data logger system---MX100

    From: Yokogawa

2. Thermocouple---Type T & Type K

    From: Chuan Chi Trading co., Ltd.

3. Digital camera---LY35862-001A

    From: JVC

4. Pressure transducer---DPG3.0

    From: Atlantis

5. Cooling circulator bath---B401H

    From: Firstek

6. Silicone glue---Permatex #82180

    From: Chuan Chi Trading co., Ltd.

7. Thermal grease---EG30

    From: Electrolube

8. Flow meter---H400M & FBCVSW50C

    From: Full Wealth Enterprise Co., Ltd.

9. Anti-fog sheet---AF001

42

From: Dr. Anti-fog

10. Condensing chamber and copper cylinders

    From: Chuan Chi Trading co., Ltd.

11. Steam generator

    From: Chuan Chi Trading co., Ltd.

3.2.2 Setup and Procedures

Equipment setup

The experimental set is shown as Figure 3-4. The copper cylinder (Figure 3-5)

was put into the chamber (Figure 3-6) with the corresponding holes on both side walls.

Seal the gaps between cylinder and chamber with the silicone glue (Figure 3-7); then

dry it for 3 hours. The aluminum container and observing window covered with

anti-fog sheet (Figure 3-8) were assembled into the condensing chamber. To be further,

the chamber was connected to the steam generator (Figure 3-9) and cooling circulator

bath (Figure 3-10) by pipe fittings and tubes.

Besides, for measuring temperatures and pressures, thermocouples and pressure

were esd in the experiments. T type of thermocouples (Figure 3-11) covered a few

thermal grease (Figure 3-12) were inserted into the holes beside the copper cylinder

while K type of them (Figure 3-13) were connected with the tees. All thermocouples

were connected to the data logger system (Figure 3-14). The pressure transducer was

43

fit into the chamber in order to measure the pressure of insider the experimental space. After connection, the experimental setup was ready for condensation.

Experimental procedures

Turn on the steam generator, cooling circulator bath with 20 ℃ setting and 50 cc/min of flow rate, and data logger system with the valve between the generator and chamber closed. Then wait for the water achieving boiling. As the temperatures of the cylinder and steam generator reached stable value, the valve was opened to let the steam flowing into the chamber. After opening, the temperature measured would be rising dramatically with tiny droplets emerging on the surface; in the meantime, images and videos started to be recorded to compare the forming conditions between different types of cylinders. As the temperatures reached stable values, increase the flow rate with 10 cc/min to increase the subcooling degrees; then record the stable values again. By repeating the steps of controlling flow meter and recording temperatures, the subcooling degrees can be observed and recorded for all types of cylinders.

Pressure measurement

The pressures were observed during the whole experiment. In order to investigate the concentration of NCGs, Gibb-Daltion ideal gas mixture equation was utilized. In this study, the concentration of NCGs was approximately 50%~60%.

$$W = \frac{p_v - p_{sat}}{p_v} \tag{3.1}$$
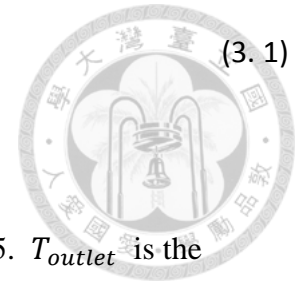
Temperature measurement and data reduction

The temperatrues measured location was shown as Figure 3-15. T_{outlet} is the

water temperature on outlet, meaning the right side, while T_{intlet} is the water

temperature on the inlet, the left side; on the other hand, T_1 to T_8 were measured to

deduce the subcooling degree ΔT_{sub}.

In order to determine ΔT_{sub}, I calculated it as the following steps. Firstly,

T_{right} and T_{left} were calculated by Equation 3.2 and 3.3, respectively, so that I

obtained the mean temperatures on both sides; then, using Equation 3.4, the heat

transported out by cooling system (Q_{water}) can be obtained by T_{outlet}, T_{inlet}, and $\dot{m}$,

the mass flow rate of cooling water measured from the flow meter.

$$T_{right} = \frac{T_1 + T_2 + T_3 + T_4}{4} \tag{3.2}$$

$$T_{left} = \frac{T_5 + T_6 + T_7 + T_8}{4} \tag{3.3}$$

$$Q_{water} = \dot{m}C_p(T_{outlet} - T_{inlet}) \tag{3.4}$$

Moveover, the heat transported in lateral direction inside the cylinder ($Q_{lateral}$)

is from Equation 3.5. k_{copper} is the thermal conductivity of copper, A_{cross} is the

cross section area of the cylinder, and Δx is the distance between the thermocouples

on two sides.

45

$$Q_{lateral} = k_{copper} * A_{cross} * \frac{(T_{left} - T_{right})}{\Delta x}$$

(3. 5)

Once the heat was decided, the average heat flux q_{avg} can be solved by

Equation 3.6 so as the wall temperature T_w by Equtaion 3.7. A_{cond} is the

condensation area, r_{tube} and r_m are radius from the central line to the outer surface

and the location of thermocouples, respectively, while L is the length of condensing

area.

$$q_{avg} = \frac{Q_{water} + Q_{lateral}}{A_{cond}}$$

(3. 6)

$$T_w = \frac{(T_{right} + T_{left})}{2} + Q_{water} \times \frac{ln\frac{r_{tube}}{r_m}}{2\pi L k_{copper}}$$

(3. 7)

At last, the subcooling degree T_{sub} and heat transfer coefficient h_{cond} can be

determined from Equation 3.8 and 3.9, respectively.

$$T_{sub} = T_s - T_w$$

(3. 8)

$$h_{cond} = \frac{q_{avg}}{T_v - T_w}$$

(3. 9)

3.3 Error Analysis

Error analysis was estimated from Taylor [72]. With the following equations, the

uncertainty of Q_{water}, $Q_{lateral}$, q_{avg}, T_{sub}, h_{cond} can be determined.

46

$$\frac{\delta Q_{water}}{Q_{water}} = \sqrt{(\frac{\delta T}{T_{outlet}-T_{inlet}})^2 + (\frac{\delta \dot{m}}{\dot{m}})^2} \qquad (3.10)$$

$$\frac{\delta Q_{lateral}}{Q_{lateral}} = \sqrt{(\frac{\delta T}{T_{right}-T_{left}})^2 + (\frac{\delta x}{x})^2} \qquad (3.11)$$

$$\frac{\delta q_{avg}}{q_{avg}} = \sqrt{(\frac{\delta Q_{water}}{Q_{water}})^2 + (\frac{\delta Q_{lateral}}{Q_{lateral}})^2} \qquad (3.12)$$

$$\frac{\delta T_{sub}}{T_{sub}} = \sqrt{(\frac{\delta T}{T_v-\frac{(T_{right}+T_{left})}{2}})^2 + (\frac{\delta Q_{water}}{Q_{water}})^2 + (\frac{\delta Q_{lateral}}{Q_{lateral}})^2} \qquad (3.13)$$

$$\frac{\delta h}{h} = \sqrt{(\frac{\delta q_{avg}}{q_{avg}})^2 + (\frac{\delta T_{sub}}{T_{sub}})^2} \qquad (3.14)$$

47

Figure 3- 5. Experimental setup.

Figure 3- 6. The copper cylinder. (L is the length of condensing area, as blue frame region is the condensation area region)

48
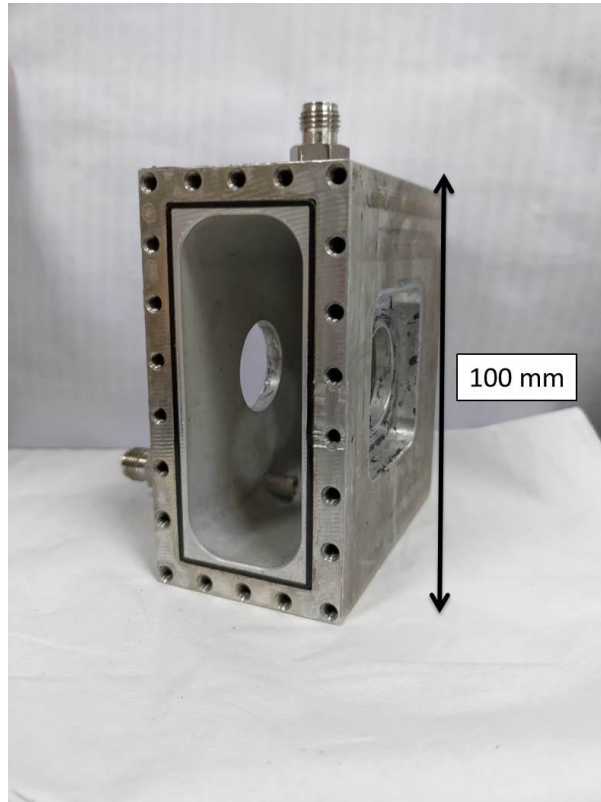
Figure 3- 7. The condensing chamber.

Figure 3- 8. The silicone glue.

Figure 3- 9. The anti-fog sheet.

Figure 3- 10. The steam generator.

Figure 3- 11. The cooling circular bath.
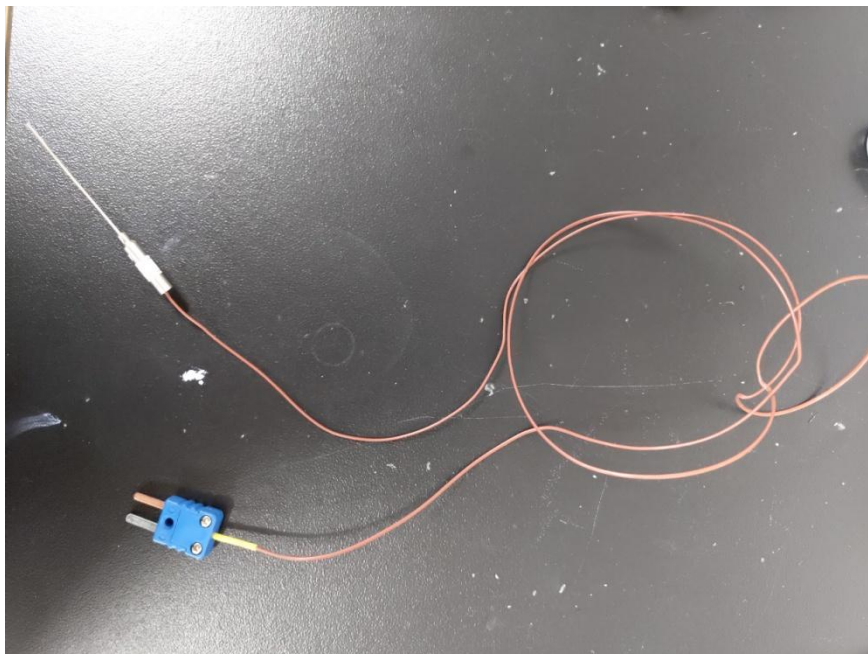
Figure 3- 12. The T type thermocouple.

51
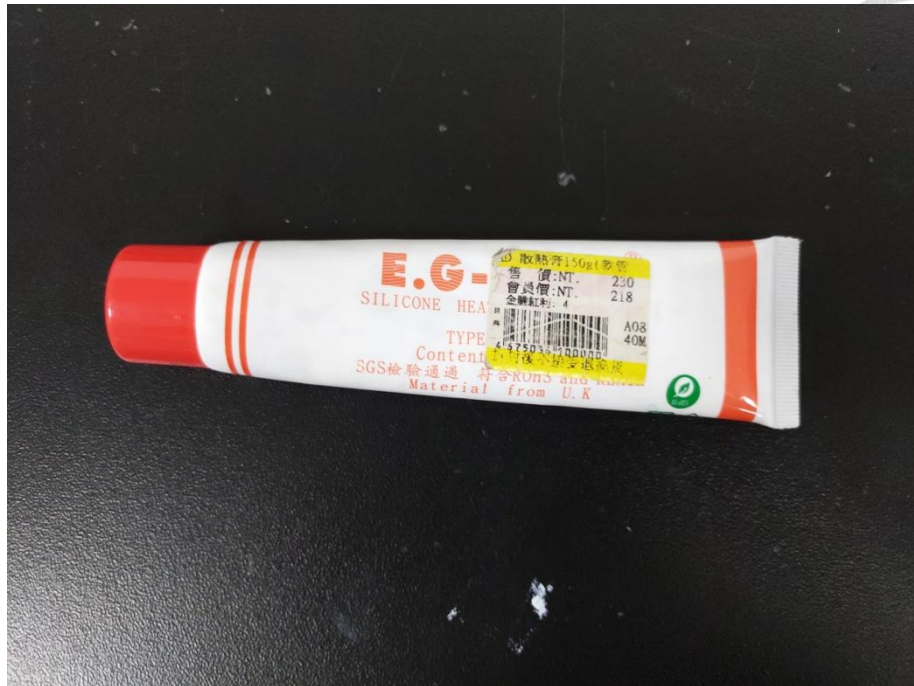
Figure 3- 13. The thermal grease.
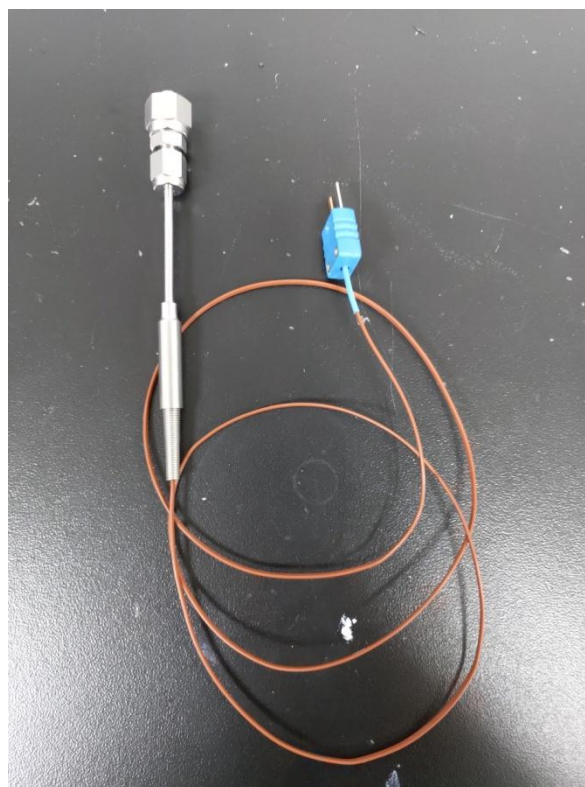
Figure 3- 14. The K type thermocouple.

52
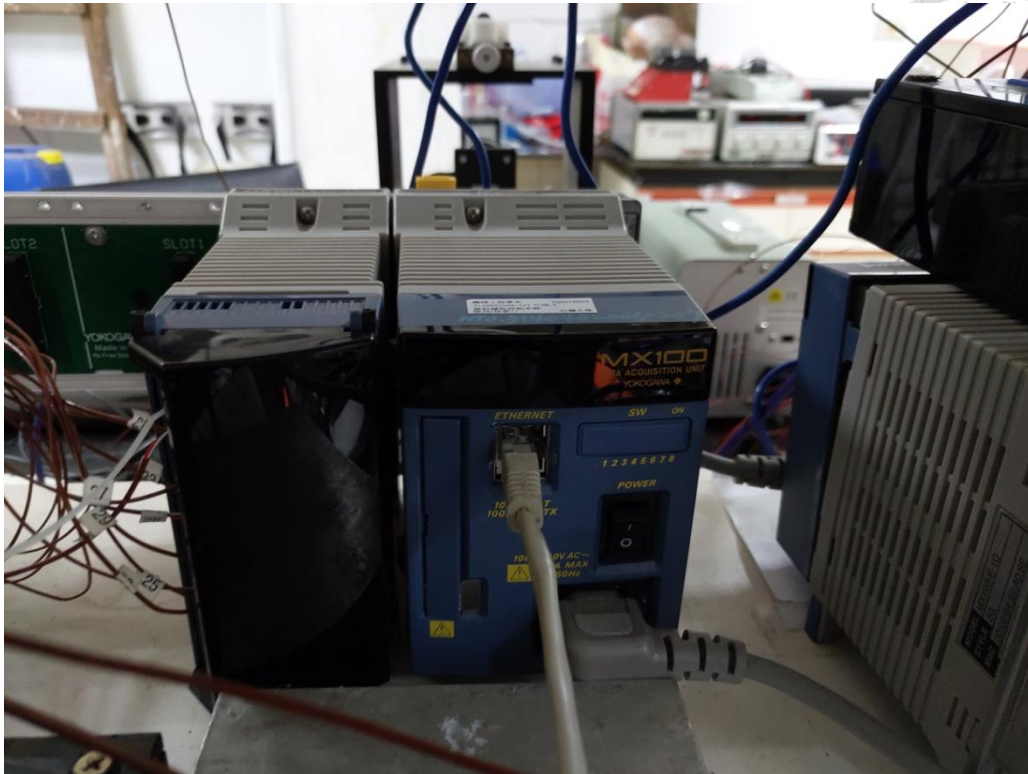
Figure 3- 15. The data logger system.
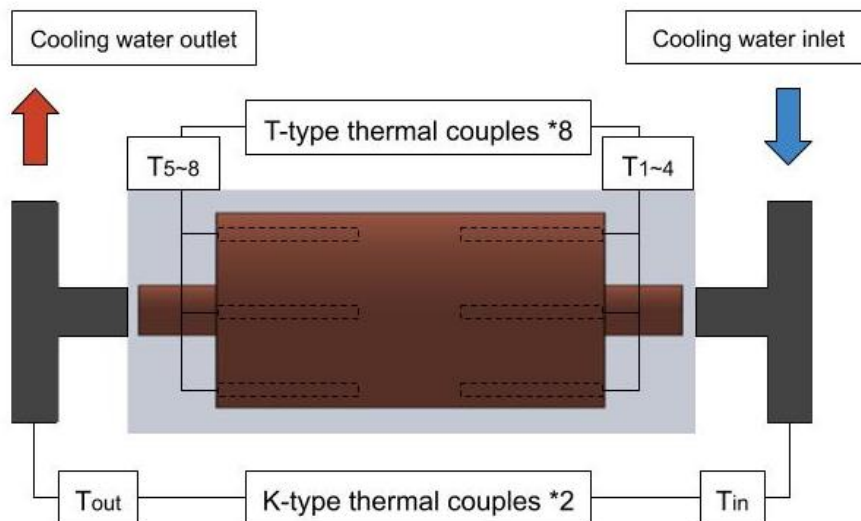
Figure 3- 16. The illustration of the temperature measured location.

Table 3- 2. The uncertainty of Q_{water}.

		Tsub (°C)		
		3	6	9
Surface types	Plain	1.46%	0.84%	0.52%
	All printed	5.01%	3.35%	2.02%
	30% printed	1.04%	0.91%	1.06%
	50% printed	1.68%	1.14%	1.16%
	70% printed	1.68%	1.28%	1.16%

Table 3- 3. The uncertainty of $Q_{lateral}$.

		Tsub (°C)		
		3	6	9
Surface types	Plain	9.09%	10.36%	11.43%
	All printed	3.45%	3.31%	2.20%
	30% printed	6.45%	7.69%	8.33%
	50% printed	3.20%	9.00%	15.38%
	70% printed	4.12%	5.26%	7.55%

Table 3- 4. The uncertainty of q_{avg}.

		Tsub (°C)		
		3	6	9
Surface types	Plain	9.21%	10.37%	11.44%
	All printed	6.08%	4.70%	2.98%
	30% printed	6.54%	7.73%	8.40%
	50% printed	3.62%	9.02%	15.43%
	70% printed	4.45%	5.42%	7.64%

Table 3- 5. The uncertainty of T_{sub}.

		Tsub (°C)		
		3	6	9
Surface types	Plain	9.53%	10.40%	11.48%
	All printed	6.62%	4.95%	3.16%
	30% printed	7.09%	7.83%	8.48%
	50% printed	4.73%	8.04%	15.45%
	70% printed	5.41%	5.63%	7.71%

Table 3- 6. The uncertainty of h_{cond}.

		Tsub (°C)		
		3	6	9
Surface types	Plain	13.25%	15.46%	16.21%
	All printed	8.99%	6.83%	4.35%
	30% printed	9.64%	10.90%	11.93%
	50% printed	5.95%	15.61%	21.83%
	70% printed	7.00%	7.81%	10.85%

Chapter 4. Results and Discussion

4.1 The Condensation Effect of CNT Printing on the Copper

At first, I investigated the effects between plain and all printed cylinders. From Figure 4-1, The heat transfer coefficient of plain copper significantly has higher values than 100% printed one during the lower interval of subcooling degrees (Tsub), which is around 0 to 7.5 ℃, while the two curves approach the steady with increasing Tsub. The declining trends result from the increasing thickness of NCGs boundary layer upon the condensing surface. The reason is illustrated as Figure 4-2. With Tsub increasing, the more heat can be transferred by the cylinder, resulting the more condensates nucleated and the less partial pressure of vapor near the condensing surface, and that is, the higher partial pressure of NCGs. In other words, the boundary layer of NCGs was getting thicker, blocking the nucleation from vapor, and inducing the rising thermal resistance.

Figure 4-1 also indicates that the heat transfer of 100% printed cylinder is not influenced by Tsub for most time. Observed from real image recorded as Figure 4-3, the condensate distribution appears as filmwise during the most interval of Tsub, while a few tiny droplets appear at lower interval. With such phenomenon, the whole values of heat transfer coefficient in 100% experiments is lower than plain ones.

56

Besides, wetting transition occurs with heat flux changes during the rise in

subcooling degree. Figure 4-4 is the condensation heat flux with changes in Tsub.

From basic heat transfer theory, the increase in Tsub corresponds to that the more heat

can be transferred, meaning the more heat flux from condensation. However, the more

heat flux induces the higher nucleation density on the surface. This will make the

coalescence of tiny droplets happen, and the wetting condition changes from dropwise

situation into filmwise situation, which is as Miljkovic et al's observation [6]. During

this transition, heat flux changes go gentle due to nonuniform distribution of growth

and coalescence, which corresponds to 5 to 7 ℃ of the plain and 8 to 13 ℃ of the

100%. Over the transition, condensates on the surface appeared as uniform liquid film,

allowing the steady increasing heat transfer.

57
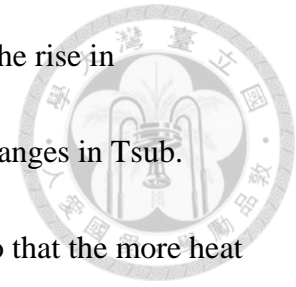
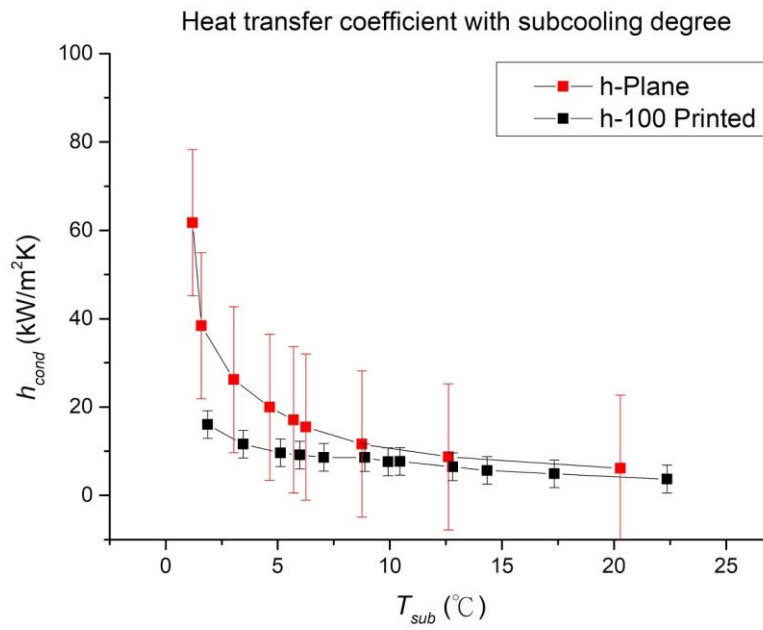Figure 4- 1. Heat transfer coefficient distribution of plain and 100% printed cylinder
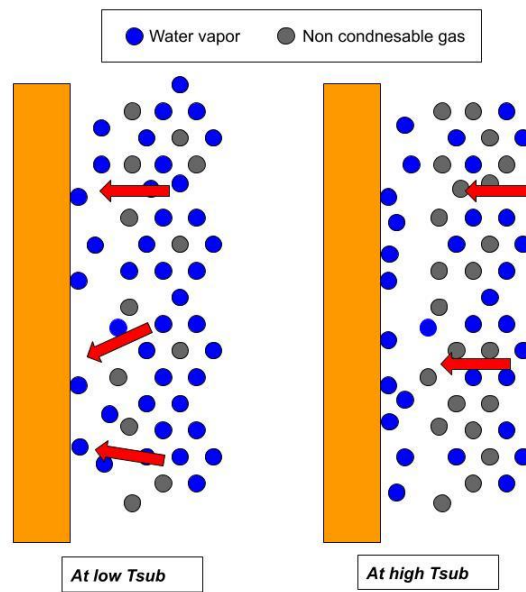with subcooling degree.

Figure 4- 2. The illustration of nucleation from vapor with changes of subcooling
degree Tsub.
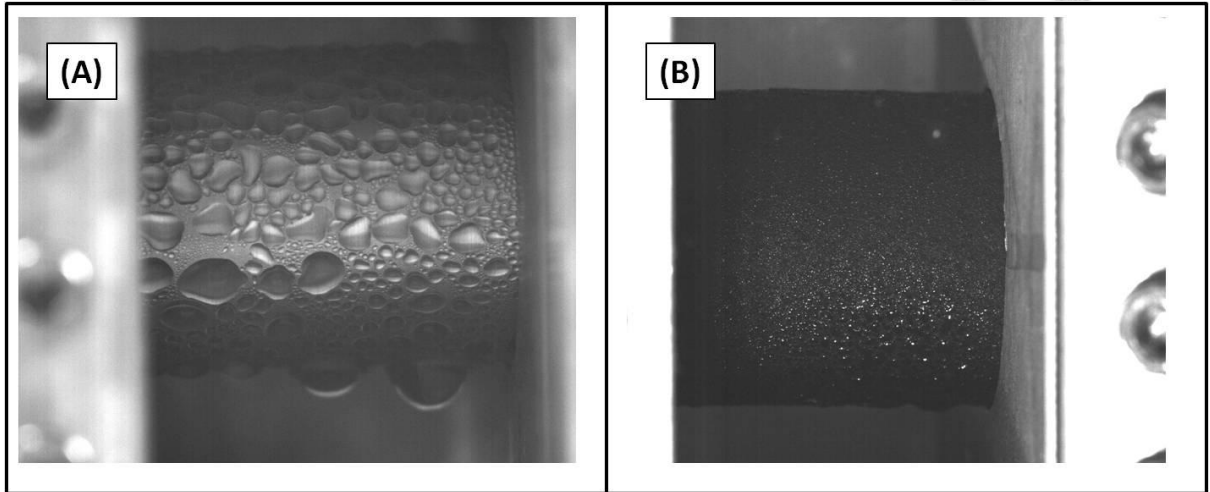
Figure 4- 3. Experimental images of plain and 100% printed copper cylinders: (A) plain (B) 100%.
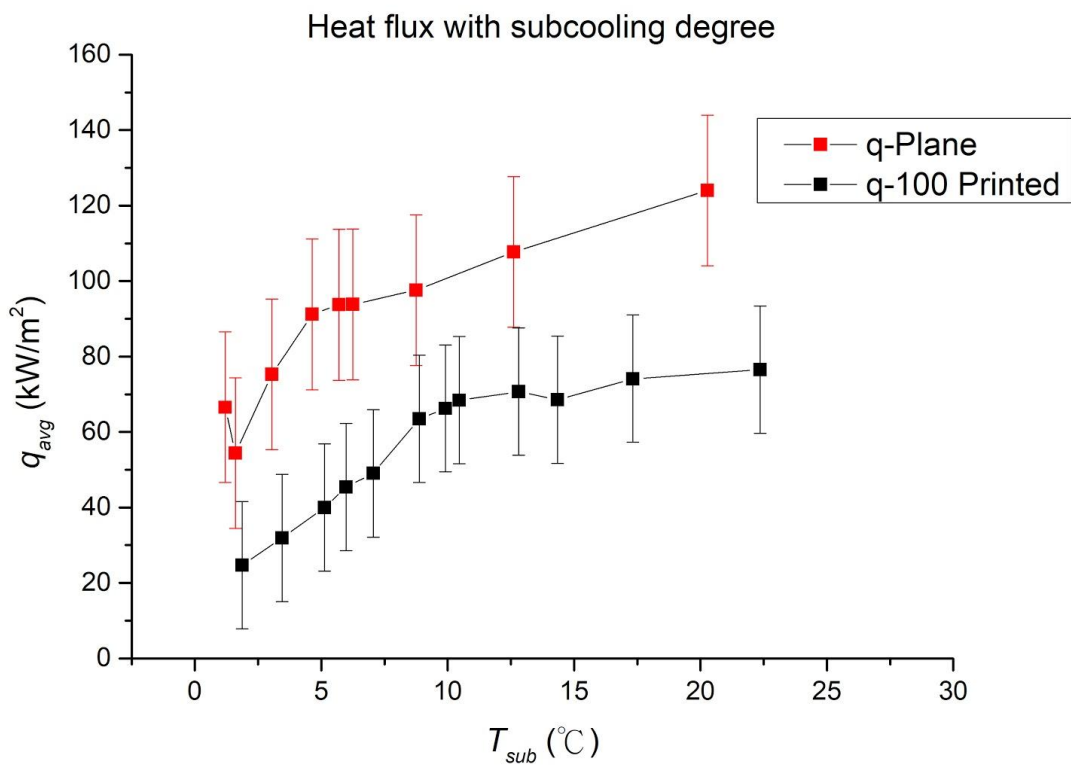
Figure 4- 4. Heat flux distribution of plain and 100% printed cylinder with subcooling degree.
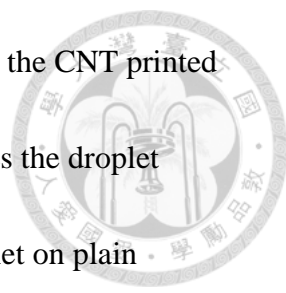
4.2 The Condensation Effect of Different Area Ratio
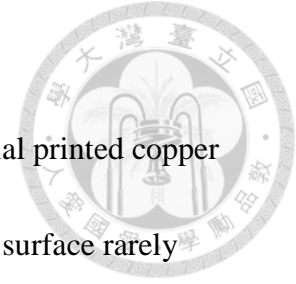
The experimental result of heat transfer coefficient for three partial printed copper cylinders is shown in Figure 4-5. The different area ratio of printed surface rarely affects the heat transfer coefficient; however, the heat flux distribution is quite different. The experimental results of heat flux for three partial printed copper cylinders is shown as Figure 4-6. At first, in the low subcooling degree (Tsub) interval, around 0 to 5 ℃, three lines show the rising trend, corresponding to the higher nucleation density changes. However, the rising trends turn into declines, and then approach steady values.

For partial printed types, the droplets size and distribution on plain surface is closely related to the droplet dynamic. In other words, the area ratios of printed and plain area to the totals affected the droplet movement. Initially at low Tsub, the plain area dominates the heat flux, so that 30% printed type has higher values than other two. During the middle interval of Tsub (around 5 to 10 ℃), the wetting transition happens on the printed and plain areas, inducing the gentle trend. As for the declines of the three types, area ratio coupled with film condensate staying on surface significantly obstructed the heat flux.

Effects of Droplets movement

60

Observed from the experimental images in Figure 4-7, because the CNT printed area is relatively hydrophilic, the increase in printed area ratio makes the droplet movement in horizontal direction more easier. As the growing droplet on plain surface attaches the condensates on printed surface, it would move toward the hydrophilic area due to surface tension, and new bare space will exist for the next nucleation. Because of this phenomenon, the more plain area leads to the less coalescence of droplets toward the printed area, and the more growth of droplets on the plain area. However, as increase in Tsub, nucleation density is coupled with the effect of printed area ratio.

Effects of nucleation changes and wetting transition

For the 30%, less droplets moved into printed area; moreover, due to the less printed area, the 30% limited the amount of condensates to move and affected the coalescence of droplets. As for the 70%, there is less enough area for nucleation on plain surface; in other words, for most time, condensates on the cylinder appeared as the filmwise. In the interval of high Tsub, the liquid film stayed on the surface for a longer time, and was difficult to fall out, which obstructed heat transfer enhancement. For the 50%, the area ratio enhanced the heat flux transfer from 0 to 4 ℃ of Tsub, and the rise goes gentle with wetting transition happening, just as the plain and the 100%. Since the equal area of the plain and the printed, the droplets on hydrophobic

area could move toward the hydrophilic area with appropriate balance. However, with the increase of Tsub, liquid film, or the flood, fully appeared in most surface of cylinder. Furthermore, the time when liquid staying on the printed area is longer than on the plain one. That is to say the non-uniform distribution surface obstructs the heat transfer and even worsen it, corresponding to the decline on the 50% in Figure 4-7.
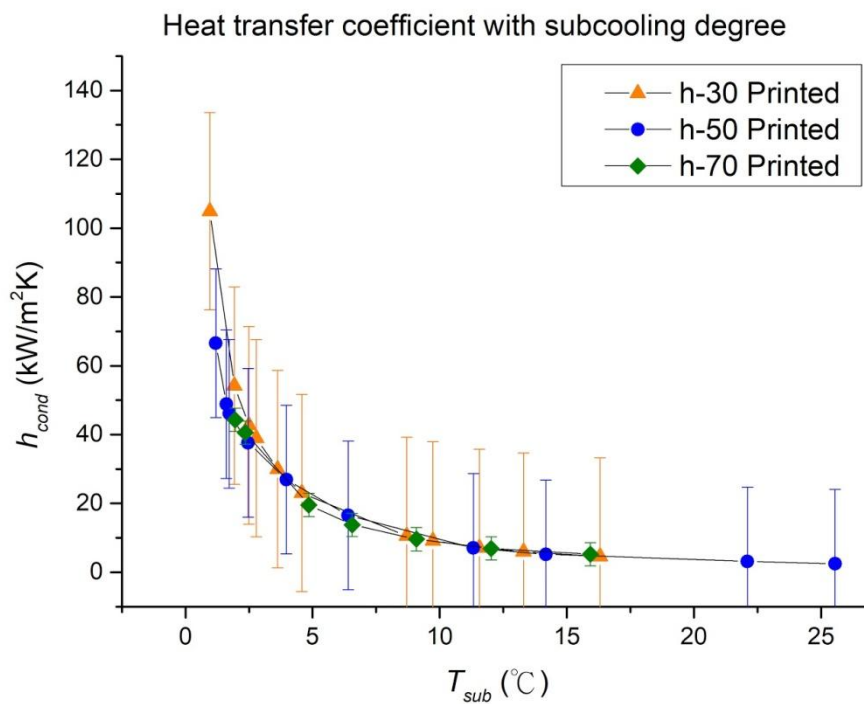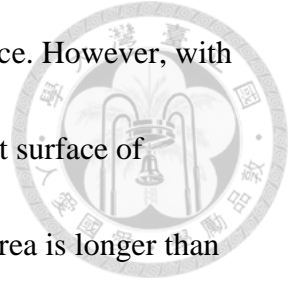

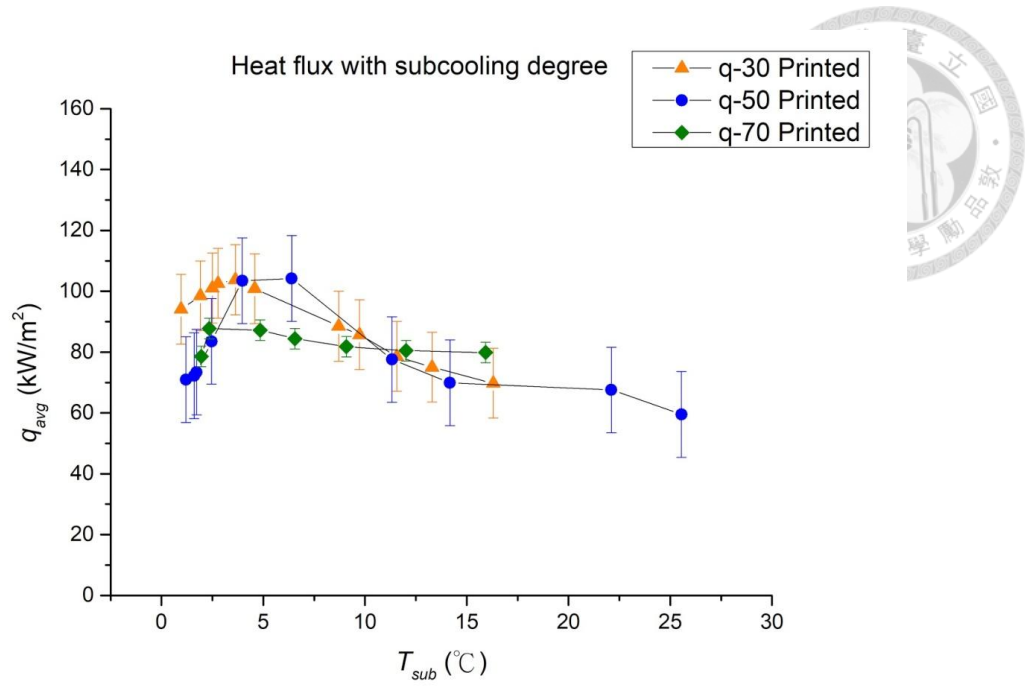Figure 4- 5. Heat transfer coefficient distribution of partial printed cylinders with subcooling degree.

Figure 4- 6. Heat flux distribution of partial printed cylinderswith subcooling degree.
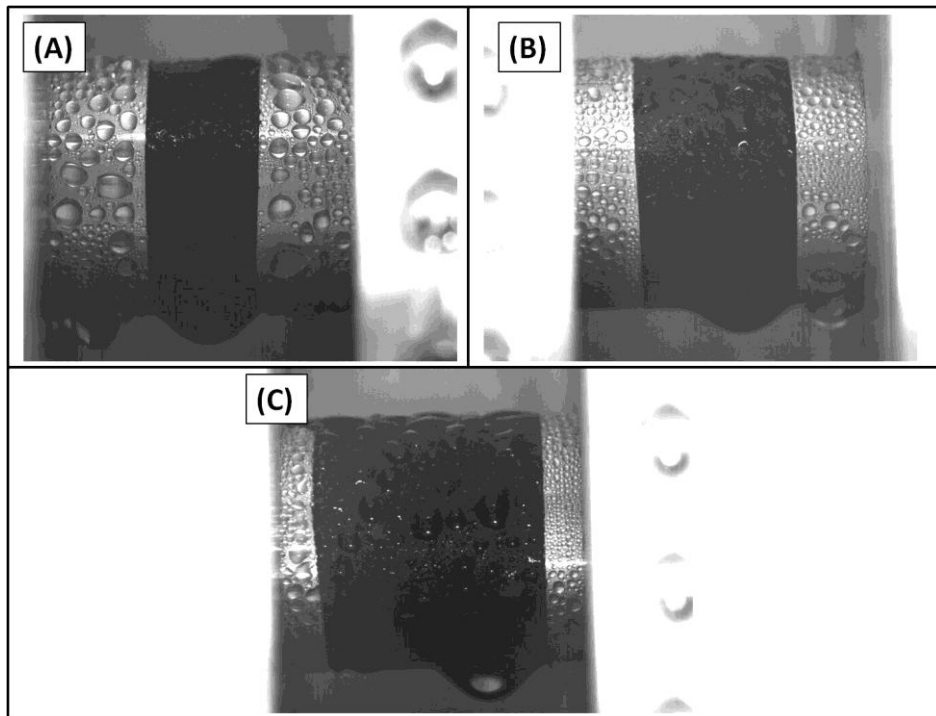
Figure 4- 7. Experimental images of partial printed copper cylinders: (A) 30%, (B) 50%, and (C) 70%.

4.3 The Discussion in Enhancement of Heat Transfer in Partial Tsub
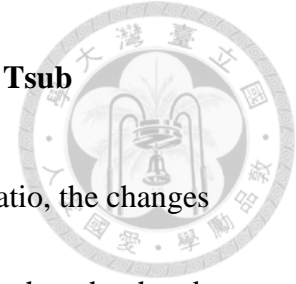
   From the discussion about the effects of CNT printing and area ratio, the changes

of heat transfer coefficient are relevant to NCGs boundary layer. On the other hands,

the changes of heat flux are associated with wetting condition and homogeneous

surface distribution. However, the values between partial types and the plain could be

explained from another aspect. Here, I discussed the comparison between plain, 30%

printed, and 100% printed types. The overall result of heat transfer coefficient (hcond)

with subcooling degree (Tsub) is shown as Figure 4-8. To be discussed in detail as

Figure 4-9, within the lower interval of Tsub (around 0 to 8 ℃), the values of the 30%

are higher than the ones of the plain. This resulted from the mechanism of disturbance

inside the NCGs boundary layer. Firstly, from Chapter 2.2.3, the coalescence and

removal of droplets would disturbs the NCGs boundary layer and make the nucleation

more easier and rapidly. In addition, the CNT printed area appears as the relatively

hydrophilic regions and motivate the movement of droplets toward this area. As

droplets form or flow near the edges of printed and plain areas, they will move into

the printed area, leading to the bare regions for the next nucleation. In the meantime,

such coalescence coupled with the removal affects the NCGs boundary layer. As a

result, there are more rapid cycles of condensation in 30% printed type than the plain

and 100% one. Besides, this disturbance also influence the heat flux changes, which is

as shown in Figure 4-10. Discussed on last part, as Tsub increased, nucleation

changes induced into wetting transition, and flood, which worsens the heat flux.
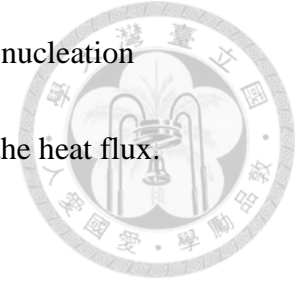
Figure 4- 8. Heat transfer coefficient distribution of plain, 30% printed, and 100% printed cylinders with subcooling degree.
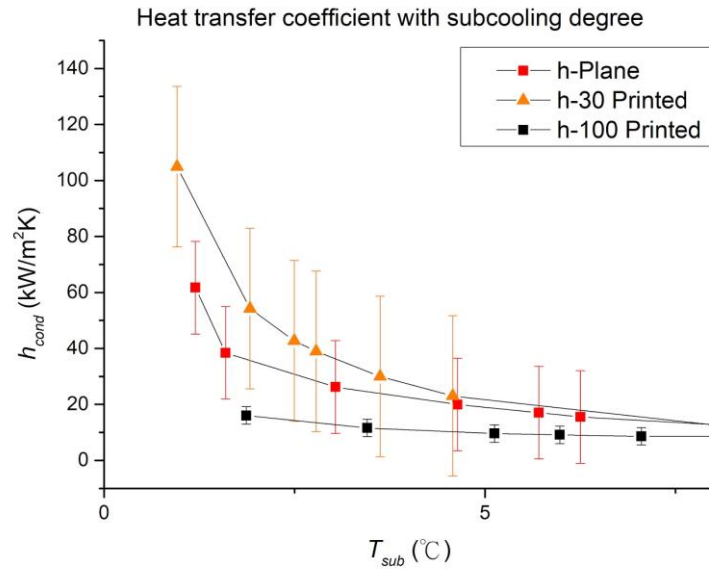
Figure 4- 9. Heat transfer coefficient distribution of plain, 30% printed, and 100% printed cylinders with subcooling degree in 0 to 8 °C.

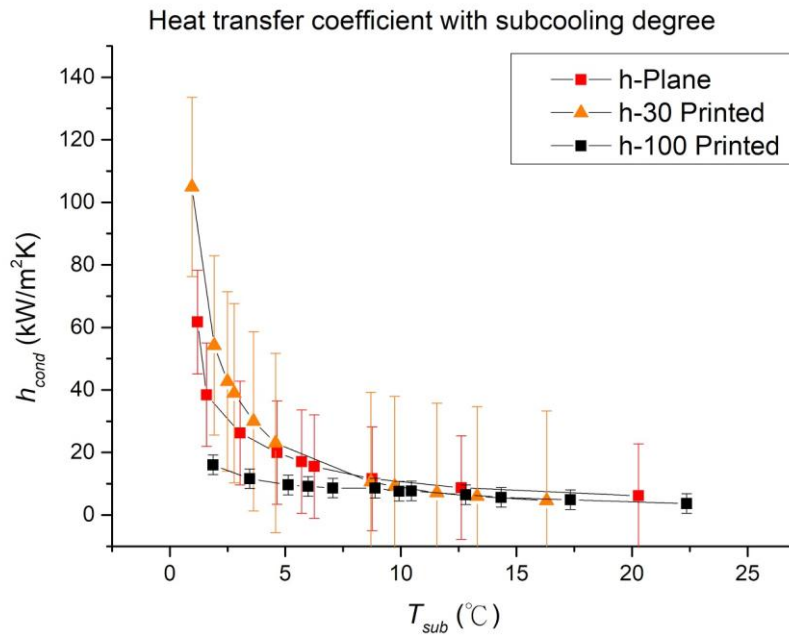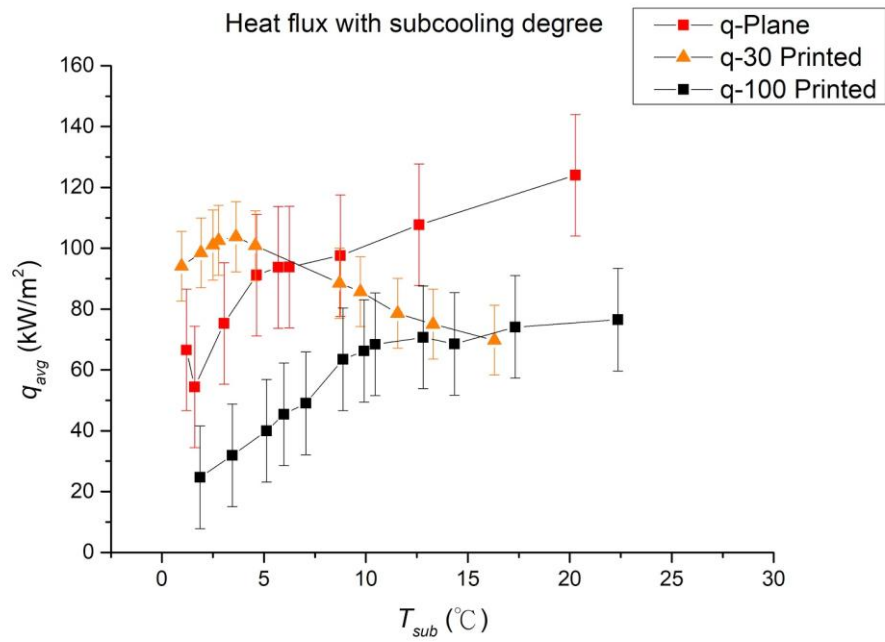Figure 4- 10. Heat flux distribution of plain, 30% printed, and 100% printed cylinders with subcooling degree.

Chapter 5. Conclusion and Future Prospects
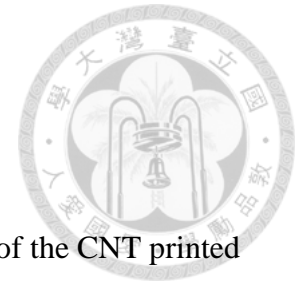
5.1 Conclusion

From the results in last chapter, the heat transfer performance of the CNT printed copper cylinder is various depending on the printed area ratio. From Figure 3-2, the CNT printed area is rough in macro-scale, which leaded to different wettability compared with lecture review [55-57]. However, the hydrophilic pattern had benefits to the heat transfer during some subcooling degrees.

For the all printed cylinder, the heat transfer coefficient and heat flux values are lower than the plain cylinder. In other words, the effects of all-CNT printing are worse due to the hydrophilic wettability. However, the declining trend with subcooling degrees is quite slowly, which means that the hydrophilic CNT printing has better stability in heat transfer performance than plain plane.

The changes in printing area ratio clearly influenced the heat performance. Firstly during low interval of subcooling degrees (0 to 5 ℃), 30% printed cylinder has higher heat transfer coefficient than other two. However, for 50% printed cylinder, the heat flux valuses stayed stable than 30% printed one in middel interval (5 to 8 ℃). As for 70% printed cylinder, the value changes are close to all printed one. Three types showed declines with high interval of subcooling in heat flux (> 8 ℃).

67

The enhancement phenomenon in heat transfer coefficient happened during the subcooling degrees from 0 to 8 ℃. The reason resulted from the hybrid area. Due to the hydrophilic area, droplet movement contains vertical and horizontal directions, which benefits the new cycle of condensation. Moreover, the coalescence and disturbs the NCGs boundary layer.
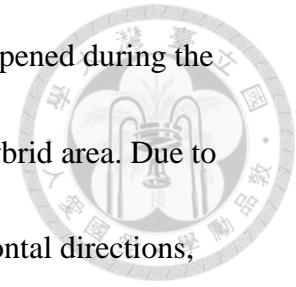
To sum up, the CNT printing is a fast way to coat on cylinder or other shapes, which could benefit the other research fields. Even the total heat transfer performance of CNT printed cylinder is worse than plain one, partial enhancement shows the CNT material has potential for improvement.

5.2 Future Prospects

Condensation heat transfer is a field worth research. Based on this study of CNT printed cylinder, the future prospects are shown as following.

1. The wettability of CNT modification on copper material could be improved by means of post processing, such as annealing, laser treatments, and so on.

2. The atmosphere of condensation in this study is not perfect for heat transfer. If the concentration of NCGs decreases, the heat flux would accordingly increase .
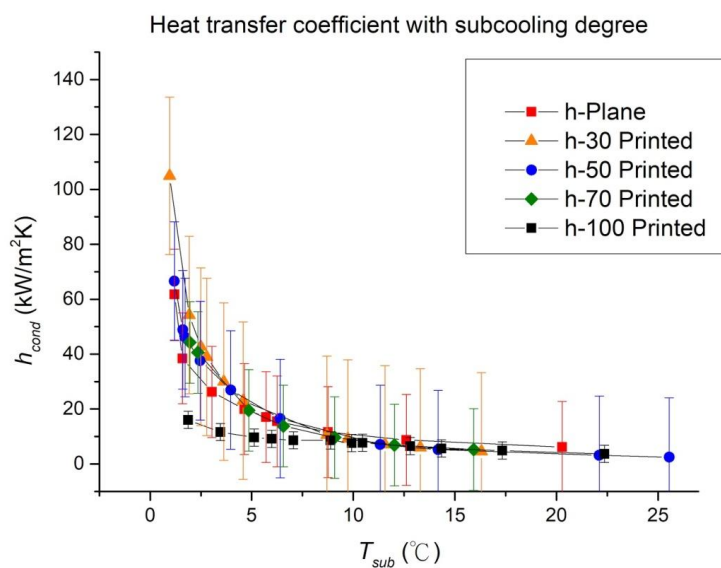
Figure 5- 1. Heat transfer coefficient distribution of all cylinders with subcooling degree.
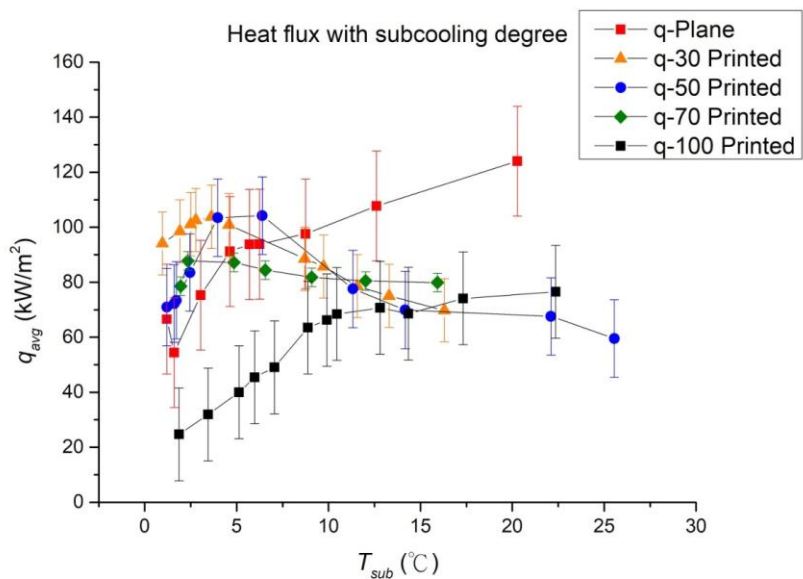
Figure 5- 2. Heat flux distribution of all cylinders with subcooling degree.

69

Reference
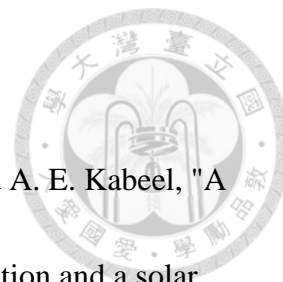
[1] S. W. Sharshir, G. Peng, N. Yang, M. O. A. El-Samadony, and A. E. Kabeel, "A continuous desalination system using humidification - dehumidification and a solar still with an evacuated solar water heater", *Applied Thermal Engineering*, vol. 104, pp. 734-742,2016.

[2] J. M. Beer, "High efficiency electric power generation: The environmental role", *Progress in Energy and Combustion Science*, vol. 33, pp. 107-134, 2007.

[3] G. Jin, K. S. Lee, and B. Seo, "Characteristics of condensation formation on the surfaces of air conditioning indoor units", Applied Thermal Engineering, vol. 91, pp. 345-353, 2015.

[4] E. Schmidt, W. Schurig, and W. Sellschopp, "Condensation of water vapour in film and drop form", *Zeitschrift Des Vereines Deutscher Ingenieure*, vol. 74, pp. 544-544, 1930.

[5] J. W. Rose, "Dropwise condensation therory and experiment: a review", *Proceedings of the Institution   of Mechanical Engineers Part a-Journey of Power and Energy*, vol. 216, pp. 115-128, 2002.

[6] N. Miljkovic, R. Enright, Y. Nam, K. Lopez, N. Dou, J. Sack, and E. N. Wang, "Jumping-droplet-enhanced condensation on scalable superhtfrophobic nanostructured surfaced", *Nano-Letters*, vol. 13, pp. 179-187, 2013.

70

[7] Y. A. Lee, L. S. Kuo, T. W. Su, C. C. HSU, and P. H. Chen, "Orientation effects

of nanoparticle-modified surfaces with interlaced wettability on condensation heat

transfer", *Applied Thermal Engineering*, vol. 28, pp. 1054-1060, 2016.
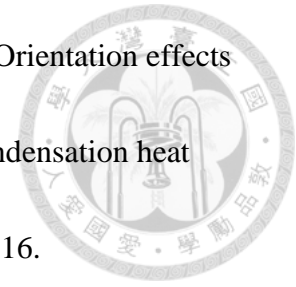
[8] J. L. Oestreich, C. W. M. van der Geld, J. L. G. Oliveria, and A. K. da Silva,

"Experimental condensation study of vertical superhydrophobic surfaces assisted by

hydrophilic constructal-like patterns", *International Journal of Thermal Sciences*, vol.

135, pp. 319-330, 2019.

[9] S. H. Hoening and R. W. Bonner, III, "Dropwise condensation on

superhydrophobic microporous wick structures", *Journal of Heat Transfer*, vol. 140,

pp. 071501-1-071501-7, 2018.

[10] A. Bachtold, P Hadley, T Nakanishi, and C. Dekker, "Logic circuits with carbon

nanotube transistors', *Science*, vol. 294, pp. 1317-1320, 2001.

[11] T. Qiao, C. M. Li, S. J. Bao, and Q. L. Bao, "Carbon nanotube/polyaniline

composite as anode material for microbial fuel cells",   Journal of Power Sources, vol.

170, pp. 79-84, 2007.

[12] E. J. Le Fevre and J. W. Rose, "A theory of heat transfer by dropwise

condensation", *Proceedings of the Third International Heat Transfer Conference*,

vol. 2, pp. 362-375, 1966.

[13] J. W. Rose, "Condensation heat transfer", *Heat Mass Transfer*, vol. 6, pp.

479-485, 1999.

[14] C. Neinhuis and W. Barthlot, "Characterization and distribution of water-repellent, self-cleaning plant surfaces", *Annals of Botany*, vol. 79, pp. 667-677, 1997.

[15] Q. Zhao, D. C. Zhang, and J. F. Lin, "Surface materials with dropwise condensation made by ion implantation technology", *Heat Mass Transfer*, vol. 34, pp. 2833-2835, 1991.

[16] D. Oner and T. J. McCarthy, "Ultrayhydrophobic surface. Effects of topography length scales on wetability", *Langmuir*, vol. 23, pp. 7293-7298, 2007.

[17] A. T. Paxson, J. L. Yague, K. K. Gleason, and K. K. Varanasi, "Stable dropwise condensation for enhancing heat transfer vis the initiated chemical vapor deposition (iCVD) of grafted polymer films", *Advanced Maerials*, vol. 26, pp. 418-423, 2014.

[18] J. Bravo, L. Zhai, Z. Z. Wu, R. E. Cohen, and M. F. Rubner, "Transparent superhydrophobic films based on silica nanoparticles", *Langmuir*, vol. 23, pp. 7293-7298, 2007.

[19] D. W. Tanner, D. West, D Pope, and C. J. Potter, "Promotion of dropwisecondensation by monolayers of radioactive fatty acids .I, stearic acid on copper surfaces", *Journet of Applied Chemistry*, vol. 14, pp. 361-369, 1964.

[20] K. M. Holden, A. S. Wanniarachchi,P J. Marto, D. H. Boone, and J. W. Rose,
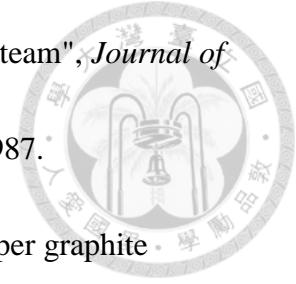
"The useof organic coatings to promote dropwise condensation of steam", *Journal of Heat Transfer-Transactions of the ASME*, vol. 109, pp. 768-774, 1987.

[21] A. Taniguchi and Y. H. Mori, "Effeciveness of composite copper graphite fluoride platings for promoting dropwise condensation of steam - a Preliminary-Study", *International Communications in Heat and Mass Transfer*, vol. 21, pp. 619-627, 1994.

[22] R. Gupta, V. Vaikuntanathan, and D. Sivakumar, "Superhydrophobic qualities of an aluminum surface coated with hydrophobic solution NeverWet", *Colloids and Surfaces A: Physicochemical and Engineering Aspects*, vol. 500, pp. 45-53, 2016.

[23] A. V. Rao, S. S. Latthe, S. A. Mahadik, and C. Kappenstein, "Mechanically stable and corrosion resistant superhydrophobic so-gel coatings on copper substrate", *Applied Surface Science*, vol. 257, pp. 5772-5776, 2011.

[24] S. Vemuri, K. J. Kim; B. D. Wood, S. Govindaraju, and T. W. Bell, "Long term testing for dropwise condensation using self-assembled monolayer coatings of n-octadecyl mercaptan", *AppliedThermal Engineering*, vol. 26, pp. 421-429, 2006.

[25] S. Vemuri and K. J. Kim, "An experimental and theoretical study on the concept of dropwise condensation", *International Journal of Heat and Mass*, vol. 49, pp. 649-657, 2006.

[26] B. Mondal, M. M. G. Eain, Q. F. Xu, V. M. Egan, J. Punch, and A. M. Lyons,

"Design and fabrication of a hybrid superhydrophobic-hydrophilic surface that exhibits stable dropwise condensation", *ACS Applied Materials & Interfaces*, vol. 7, pp. 23575-23588, 2015.

[27] J. Shim, D. Seo, S. Oh, J. Lee, and Y. Nam, "Condensation heat-transfer performance of thermally stable superhydrophobic cerium-oxide surfaces", *ACS Applied Materials & Interfaces*, vol. 10, pp. 31765-31776, 2018.

[28] R. D. Narhe and D. A. Beysens, "Growth dynamics of water drops on a square-pattern rough hydrophobic surface", *Langmuir*, vol. 23, pp. 6486-6489, 2007.

[29] C. Dorrer and J. Ruhe, "Condensation an wetting transitions on microstructured ultrahydrophobic surfaces", *Langmuir*, vol. 23, pp. 3820-3824, 2007.

[30] C. Dorrer and J. Ruhe, "Some thoughts on superhydrophibic wetting", *Soft Matter*, vol. 5, pp. 51-61, 2009.

[31] C. P. Migliaccio, "Resonance-induced condensate shedding for high-efficiency heat transfer", *International Journal of Heat and Mass Transfer*, vol. 79, pp. 720-726, 2014.

[32] W. Lei, Z. H. Jia, J. C. He, T. M. Cai, and G. Wang, "Vibration-induced Wenzel Cassie wetting transition on mircostructured hydrophobic surfaces", *Applied Physical Letters*, vol. 104, pp. 181601, 2014.

[33] E. Bormashenko, R. Pogreb, G. Whyman, and M. Erlich, "Resonence

Cassie-Wenzel wetting transtion for horizontally vibrated drops deposited on a rough

surface", *Langmuir*, vol. 23, pp. 12217-12221, 2007.

[34] J. Bravo and C. H. Chen, "Restoring superhydrophobicity of lotus leaves with

vibration-induced dewetting", *Physical Review Letters*, vol. 103, 174502, 2009.

[35] M. Washizu, "Electrostatic actuation of liquid droplets for microreactor

applications", *IEEE Transactions on industrial application*, vol. 34, pp. 732-737,

1998.

[36] C. H. Chen, Q. J. Cai, C. L. Tsai, C. L. Chen, G. Y. Xiong, Y. Yu, and Z. F. Ren,

"Dropwise condensation on superhydrophobic surfaces with two-tier roughness",

Apllied Physical Letters, vol. 90, 173108, 2008.

[37] J. B. Boreyko and C. H. Chen, "Self-propelled dropwise condensate on

superhydrophobic surfaces", *Physical Review Letters*, vol. 103, 184501, 2009.

[38] J. T. Cheng, A. Vandadi, and C. L. Chen, "Condensation heat transfer on two-tier

superhydrophobic surfaces". *Applied Physical Letters*, vol. 101, 131909, 2012.

[39] X. Yan, L. Zhang, S. Sett, L. Feng, C. Zhao, Z. Huang, H. Vahabi, A. K. Kota, F.

Chen, and N. Miljkovic, "Droplet jumping: effects of droplet size, surface structure,

pinning, and liquid properties", *ACS Nano*, vol. 13, pp. 1309-1323, 2019

[40] R. Enright, N. Miljkovic, A. Al-Obeidi, C. V. Thompson, and E. N. Wang,

"Condensation on superhydrophobic surfaces: the role of local energy barriers and

structure length scale", *Langmuir*, vol. 28, pp. 14424-14432, 2012.

[41] K. Rykaczewski, W. A. Osborn, J. Chin, M. L. Walker, J. H. Scott, W. Jones, C. L. Hao, S. H. Yao, and Z. K. Wang, "How nanorough is rouigh enough to make a surface superhydrophobic during water condensation?", *Soft Matter*, vol. 8, pp. 8786-8794, 2012.

[42] A. Chatterjee, M. M. Derby, Y. Peles, and M. K. Jensen, "Enhancement of condensation heat transfer with patterned surfaces", *International Journal of Heat and Mass Transfer*, vol. 71, pp. 675-681, 2014.

[43] A. M. Macner, S. Daniel, and P. H. Steen, "Condensation on surface energy gradient shifts drop size distribution toward small drops", *Langmuir*, vol. 30, pp. 1788-1798, 2014.

[44] B. L. Peng, X. H. Ma, Z. Lan, W. Xu, and R. F. Wen, "Experimental investigation on steam condensation heat transferenhancementwith vertically patterned hydrophobic-hydrophilic hybrid surfaces", *International Journal of Heat and Mass Transfer*, vol. 83, pp. 27-38, 2015.
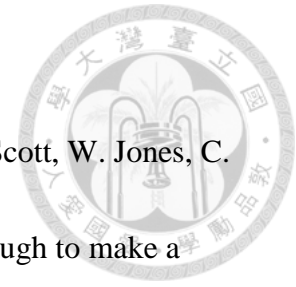
[45] A. Ghosh, R. Ganguly, T. M. Schutzius, and C. M. Megaridis, "Wettability patterning for high-rate, pumpless fluid transport on open, non-planar microfluidic platforms", *Lab on a Chip*, vol. 14, pp. 1438-1550, 2014.

[46] A. Ghosh, S. Beaini, B. J. Zhang, R. Ganguly, and C. M. Megaridis, "Enhancing

dropwise condensation through bioinspired wettability patterning", *Langmuir*, vol. 30,

pp. 13103-13115, 2014.
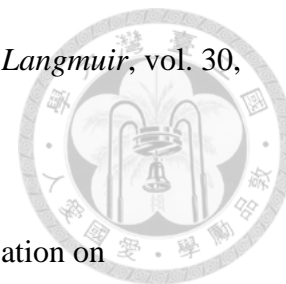
[47] M. Alwazzan, K. Egab, B. Peng, J. Khan, and C. Li, "Condensation on

hybrid-patterned copper tubes (I): Characterization of condensation heat transfer",

International Journal of Heat and Mass Transfer, vol. 112, pp. 991-1004, 2017.

[48] S. Pacchini., K. Frigui, C.-A. Paragua, E. Flahaut, S. Bila, B.K. Tay, and D.

Baillargeat, "CNTs effects on RF resonator printed on paper", *IEEE MTT-S*

International Microwave Symposium Digest, 10.1109/MWSYM.6697794. 2013.

[49] H. Jing, Y. Jiang, and X. Du, "Screen-printed single-walled carbon nanotube

networks and their use for dimethyl methylphosphonate detection", Journal of

Materials Science: Materials in Electronics, vol. 23, pp. 1823-1829, 2012

[50] D. Janczak, M. Słoma, G. Wróblewski, A. Młożniak, and M. Jakubowska,

"Screen-printed resistive pressure sensors containing graphene nanoplatelets and

carbon nanotubes", Sensors, vol. 14, pp. 17304-17312, 2014

[51] H. Menon, R. Aiswaryaab, and K. P. Surendran, "Screen printable MWCNT inks

for printed electronics", *RSC Adv.*, 44076-44081, 2017.

[52] A. M. Marconnet , M. Motoyama , M. T. Barako, Y. Gao, S. Pozder, B. Fowler,

K. Ramakrishna, G. Mortland, M. Asheghi, and K. E. Goodson, "Nanoscale

conformable coatings for enhanced thermal conduction of carbon nanotube films",

77

13th InterSociety Conference on Thermal and Thermomechanical Phenomena in Electronic Systems, pp. 15-19, 2012.

[53] G.-M. Vallet, M. Dunand, and J.-F. Silvain, "Influence of carbon nanotubes dispersion on thermal properties of copper-carbon nanotubes (CNTs) composite materials", *Universal Journal of Materials Science*, vol. 3, pp. 55-61, 2015.

[54] R. K. Bera, S. G. Mhaisalkar, D. Mandler, and S. Magdassi, "Formation and performance of highly absorbing solar thermal coating based on carbon nanotubes and boehmite", *Energy Conversion and Management*, vol. 120, pp. 287-293, 2016.

[55] C. Journet, S. Moulinet, C. Ybert, S. T. Purcell, and L. Bocquet, "Contact angle measurements on superhydrophobic carbon nanotube forests : effect of fluid pressure", *Europhysics Letters*, vol. 71, pp. 104-109, 2005.

[56] A. Aria, and M. Gharib, "Physicochemical characteristics and droplet impact dynamics of superhydrophobic carbon nanotube arrays", Langmuir, vol. 30, pp. 6780-6790, 2014.

[57] A. I. Aria and M. Gharib, "Reversible tuning of the wettability of carbon nanotube arrays: the effect of ultraviolet/ozone and vacuum pyrolysis treatments", *Langmuir,* vol. 27, pp. 9005-9011, 2011.

[58] P. M. Masipa, T. Magadzu, and B. Mkhondo, "Decoration of Multi-walled Carbon Nanotubes by Metal Nanoparticles and Metal Oxides using Chemical

Evaporation Method", *South African Journal of Chemistry*, vol. 66, 2013.

[59] S. Park, M. Vosguerichian, and Z. Bao, "A review of fabrication and applications of carbon nanotube film-based flexible electronics", NANOSCALE, vol. 5, pp. 1727-1752, 2013.

[60] S. Ditrich, "Wetting phenomena", *Phase Transitions and Critical Phenomena*, vol. 12, pp. 1-218, 1988.

[61] R. N. Wenzel, "Resistance of solid surfaces to wetting by water", *Industrial and Engineering Chemistry*, vol. 28, pp. 988-994, 1936.

[62] A. Lafuma and D. Quere, "Superhydrophobic states", *Nature Materials*, vol. 2, pp. 457-460, 2003.

[63] A. B. D. Cassis and S. Baxter, "Wettability of porous surfaces", *Transitions of the Faraday Society*, vol. 40, pp. 0546-0550, 1994.

[64] N. Miljkovic, R. Enright, and E. N. Wang, "Effect of droplet morphology on growth dynamics and heat transfer during condensation on superhydrophobic nanostructured surfaces", ACS Nano, vol. 37, pp. 4965-4970, 1988.

[65] E. Bormashenko, "Wetting of real solid surfaces: new blance on well-known problems", Colloid and Polymer Science, vol. 291, ppt. 339-342, 2013.

[66] Q. S. Zheng, Y. Yu, and Z. H. Zhao, "Effects of hydraulic pressure on the stability ad ytransition of wetting modes of surperhydrophobic surfaces", American

Chemical Society Journals, vol. 21, pp. 12207-12212, 2005.
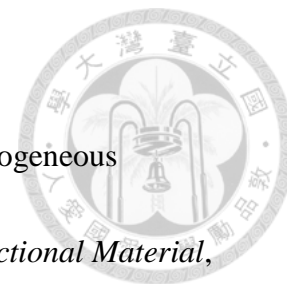
[67] C. W. Lo, C. C. Wang, and M. C. Lu, "Spatial control of heterogeneous nucleation on the superhdrophobic nanowire array", *Advanced Functional Material*, vol. 24, pp. 1211-1217, 2014.

[68] D. Beysens, "The formation of dew", *Atmospheric Research*, vol. 39, pp. 215-237, 1995.

[69] B. H. R. Talesh and S. Hamid, "Theoretical study of stable dropwise condensation on an inclined micro/nano-structured tube", *International Journal of Refrigeration*, vol. 75, pp. 322-328, 2016.

[70] X. H. Ma, X. D. Zhou, Z. Lan, Y. M. Li, and Y. Zhang, "Condensation heat transfer enhancement in the presence of non-condensable gas using the interfacial effect of dropwise condensation", *International Journal of Heat and Mass Transfer*, vol. 51, pp. 1729-1737, 2008.

[71] R. Wen, X. Zhou, B. Peng, Z. Lan, R. Yang, and X. Ma, "Falling-droplet enhanced filmwise condensation in the presence of non-condensable gas", *International Journal of Heat and Mass Transfer*, vol. 140, pp. 173-186, 2019.

[72] J.R Taylor, *An introduction to error analysis: the study of uncertainties in physical measurements, 2nd Ed.* Sausalito, California: University Science Books, 1997.